

Numerical simulations of excess enthalpy geothermal wells

By

Daníel Bergur Ragnarsson

A Master's Thesis

Submitted to the Chair for Computational Geoscience, Geothermics and Reservoir Geophysics

Rheinisch-Westfälische Technische Hochschule Aachen

In Fulfilment of the Requirements

For a Master's Degree

November 2023

Abstract

Geothermal wells direct geothermal fluids from reservoir to the surface where they enable the production of power and exploitation of the heat contained therein. The specific enthalpy (vapour to liquid ratio) of that fluid determines its suitability for power production. When a geothermal well starts producing, the specific enthalpy sometimes increases beyond the initial level in an event called excess enthalpy discharge. Such wells are aptly named excess enthalpy wells and are highly valued for their potential in power production. However, the geological controls behind this process are poorly understood. To gain a better understanding of the causes of excess enthalpy discharges, 3D numerical modelling of fluid production from boiling and sub-boiling aquifers was performed. The models show that the process initiates in boiling zones, from induced boiling following depressurisation of the reservoir, phase segregation under sufficiently low fracture permeability, and under the right relative permeability conditions. EED due to spiking in enthalpy occurs at fracture permeabilities around $1e^{-15} \text{ m}^2$ for sub-boiling reservoirs. While generally, spiking in enthalpy occurs at and below $2e^{-15} \text{ m}^2$ in both types of reservoirs. Other parameters such as matrix permeability, fracture spacing, feed zone depth, matrix volume fraction, and relative permeability curves are secondary and can affect the running enthalpy curve, shifting it, changing its amplitude, or alter the enthalpy spike frequency in tight fractured reservoirs, but do not induce or prevent excess enthalpy discharges from forming under the appropriate primary conditions.

List of contents

Abstract.....	2
List of contents.....	3
List of abbreviations.....	4
Acknowledgements.....	5
1. Introduction.....	6
1.1 Background.....	7
1.1.1 Excess enthalpy discharges.....	7
1.1.2 Well measurements.....	7
1.1.3 Steam cap development.....	7
1.1.4 Dual porosity modelling.....	8
1.2 Objective.....	8
2. Methods.....	10
2.1 Governing equations.....	10
2.2 Model Setup.....	13
2.3 Natural state.....	15
2.4 Simulation approach.....	15
3. Results.....	16
3.1 Natural state.....	16
3.2 Base case.....	17
3.3 Controls on well discharge enthalpy.....	18
3.3.1 Fracture permeability.....	18
3.3.2 Matrix permeability.....	19
3.3.3 Fracture spacing.....	21
3.3.4 Depth of feed zone.....	22
3.3.5 Matrix volume fraction.....	24
3.3.6 Relative permeability curves.....	25
3.4 Impact of production on reservoir.....	26
4. Discussion.....	30
Citations.....	33

List of abbreviations

BHP	Bottom Hole Pressure
EED	Excess Enthalpy Discharge
IDE	Initial Discharge Enthalpy
IRE	Initial Reservoir Enthalpy
REV	Representative Elementary Volume

Acknowledgements

I'd like to thank my parents and in-laws that supported me during the entire process of simulating and writing.

I'd like to express my gratitude to my supervisor, Samuel Warren Scott, for his topic suggestion and all his invaluable insight into numerical simulations of geothermal systems. His passion for the subject and talent for explaining it in understandable terms made this a very enjoyable project.

Moreover, I'd like to extend special thanks to Dr. Peter Franz and Dr. Jonathon Clearwater at Flow State Solutions for providing me with access to their simulation suite 'Volsung', which allowed for a powerful integration between reservoir and wellbore modelling that proved essential to the work in this thesis.

And finally I'd like to thank my wife, Marie, who really loves hot water.

1. Introduction

Geothermal energy is a suitable alternative to fossil fuels when it comes to energy production due to its relatively stable baseline of operational capacity and reduced carbon emissions compared to conventional baseload energy sources (Friðriksson et al. 2016). That makes it an important, but underutilised source of heat and energy as the world transitions into renewable energy sources. Geothermal wells harness energy from the geothermal systems by redirecting high enthalpy fluids from reservoir to turbine. The most important property of a geofluid for power production is its enthalpy. In the context of geothermal systems, enthalpy can be defined as the sum of the system's internal energy and the work done by the flowing reservoir fluid. Specific enthalpy is defined as enthalpy per unit mass (Yan, 2022). **Figure 1.1.** shows a phase diagram of pure water as a function of pressure and specific enthalpy. As the water's specific enthalpy under the two phase curve increases, the temperature stays the same due to the latent heat of liquid water, while the mass and volume fractions of vapour increase. These fractions determine the quality of the extracted fluid for power production.

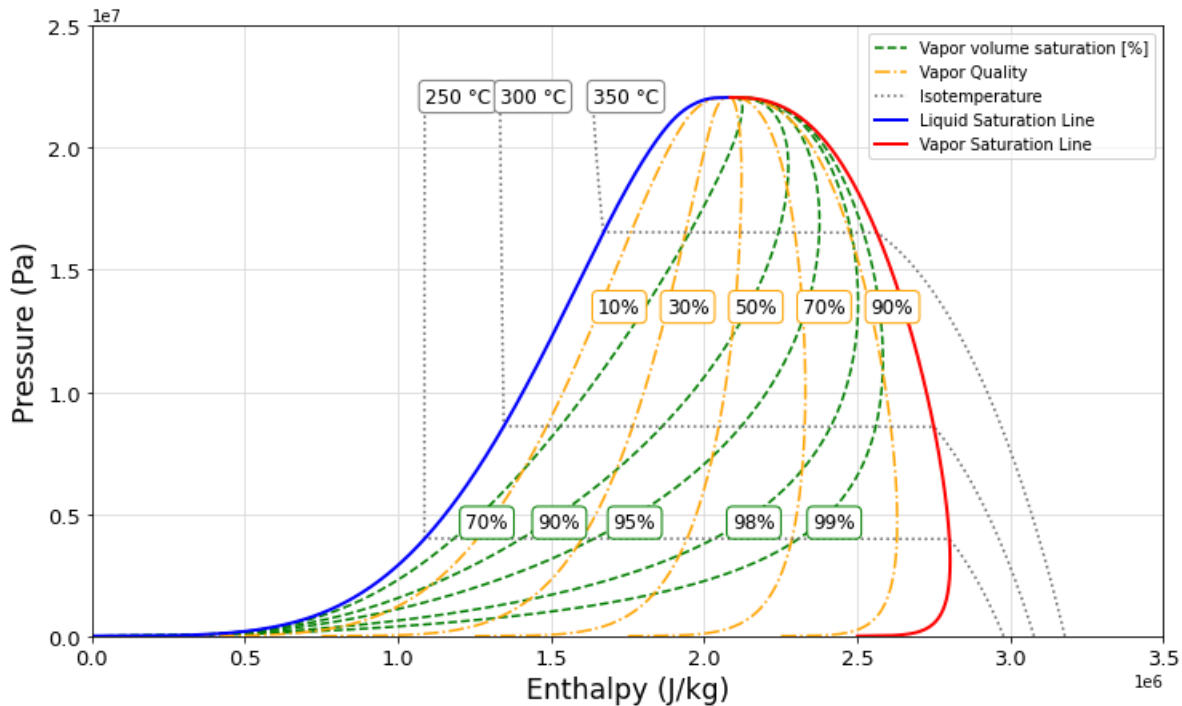


Figure 1.1: A pressure enthalpy diagram for pure water. The blue and red lines are the respective liquid and vapour saturation isolines. In grey are the temperature isolines representing equal temperatures. In green we have the vapour volume fraction in intervals from 70% to 99%. Finally we have the isolines of vapour quality or vapour mass fraction in yellow.

1.1 Background

Below is a listed description of some vital concepts for the work done in later sections of the thesis.

1.1.1 Excess enthalpy discharges

As geothermal fluids are extracted, the flowing enthalpy and pressure are expected to drop. Under certain conditions however, the flowing enthalpy of wells increases beyond the initial enthalpy discharge. This phenomenon is termed '**excess enthalpy discharge**' (shortened to EED). EED's can form through depressurisation boiling of the liquid phase in a geothermal reservoir. As the pressure drops, the superheated liquid boils off and wells can start producing dry steam such as seen in Svartsengi, Iceland, and Wairakei, New Zealand. Alternatively EEDs can form from phase segregation of vapour and liquid. Vapour has higher mobility than liquid due to multiple factors including lower density in buoyancy driven convection and lower dynamic viscosity.

1.1.2 Well measurements

Upon well completion a limited fluid flow is bled out to allow the system to thermally equilibrate and avoid thermal shock damage to its components. Then the wellhead pressure is slowly decreased and a well deliverability curve is produced by measuring the well's mass flow rate against wellhead pressure. That determines deliverability from the lowest pressure (fully open valve) to the highest pressure that still delivers fluid. For single phase fluids the enthalpy can be easily tested. Many wells however deliver a two phase mixture, whose components need to be separated and measured independently. That is a costly process both in terms of equipment required and the time where the well is not producing (Zarrouk & McLean, 2019). Alternatively enthalpy measurements are conducted using a total flow calorimeter, where the geothermal fluid is discharged into a tank of water of known volume and temperatures. From there the flow rate and enthalpy can be calculated using a mass-energy balance equation (Grant & Bixley, 2011). In general all direct methods require some sort of interruption to production and sometimes costly or time consuming setups. Running tests like natural or synthetic tracer tests can prove unreliable as small pressure changes can flash or condense the respective phases and increase or decrease concentrations of tracers with an affinity for the liquid phase (Marini and Cioni, 1985).

1.1.3 Steam cap development

Boiling zones are an important factor for the development of EEDs. Multiphase fluid flow simulations indicate that large scale permeability structures are the primary control of the formation of boiling caps in high enthalpy geothermal systems with permeability on the order of $1e^{-15} \text{ m}^2$ forming the hottest, steam rich systems. At permeabilities of $1e^{-16} \text{ m}^2$ and below, the geothermal systems become conduction dominated and exhibit modest increase in near-surface temperature. (Scott et al. 2016; Hayba and Ingebritsen 1994). Moreover, magma intrusion (heat

source) emplacement depth and cap rock thickness act as secondary controls on natural steam cap formations (Scott 2020).

Table 1.1: Descriptive designation of bulk geothermal reservoir permeability according to literature (Scott et al. 2016; Ingebritsen 1994).

Permeability	[m²]
High	1e ⁻¹⁴
Intermediate	1e ⁻¹⁵
Low	1e ⁻¹⁶

1.1.4 Dual porosity modelling

Numerical models show that dual porosity approaches are needed to reproduce the behaviour of EEDs (Austria, Jr. (2014), Austria, Jr. & O’Sullivan (2015) and Sandström (2021)), as single porosity models give a very conservative estimate on enthalpy discharge. Unlike single porosity models, where the lithological medium is assumed to be of uniform porosity and permeability, dual porosity models assume a matrix volume fraction of uniform porosity and permeability, interconnected by a smaller volume fraction fracture network that interconnects the disconnected matrix volumes. These matrix volumes can exchange mass and energy with the fracture network (Pruess, 1992).

1.2 Objective

The occurrence of excess enthalpy discharges is generally favourable from a production standpoint as they result in more steam delivered and consequently more electricity generated. However, the physical factors controlling EEDs are not well understood and as such have an impact on production in terms of confidently assessing the evolution of a well’s performance. In some cases, reservoir models are not able to reproduce the characteristics of EEDs. EEDs display transient changes where enthalpy either increases or decreases with time. As a result, understanding of the physical parameters controlling running enthalpy in geothermal wells needs to be furthered.

To gain a better understanding of the phenomenon of EED generation, I performed numerical simulations of fluid production from high temperature (250°C- 350°C) geothermal systems. This study focuses on the major natural and production factors behind EED development, namely:

1. Initial reservoir state. Specifically whether it is boiling or sub-boiling.
2. Matrix-fracture permeability contrast
3. Feed- zone depth
4. Matrix volume fraction
5. Fracture spacing
6. Relative permeability curves

These models are then used to understand which of these factors can cause short-term fluctuations in well-discharge enthalpy by means of 3D reservoir modelling using the Volsung simulation suite by Flow State Solutions.

2. Methods

The natural state models and the subsequent variations for the production phase are modelled in Flow State Solution's Volsung software suite. The package integrates a 3D graphical user interface for building models with a fast reservoir simulator, a wellbore simulator and many other geothermal simulation tools (Franz and Clearwater, 2023). The software uses the equations and formulations listed in **section 2.1**. After creating the model it is run to simulate the system's natural state, subsequently the natural state is used as a starting point for all following production stage simulations.

2.1 Governing equations

The reservoir heat and fluid flow is calculated using the MINC method which is short for Multiple Interacting Continua. Developed by Pruess and Narasimhan in the 1980s, this model treats pore permeability and fracture permeability as separate elements that interact with each other. The matrix blocks are set to be slowly invaded by changing reservoir conditions, while the fracture network is quickly affected due to higher permeability. Moreover, unlike conventional dual porosity models, MINC discretizes the pore volumes into 'layers', with the first layer being the fractures, the second the proximal matrix pore volume to the fractures and any subsequent layer representing a more distal volume of the pore matrix. Using only two layers reduces the MINC model to a simple dual porosity model. (Pruess, 1992). The fluid flow follows Darcy's law (**Eqts 2.1 & 2.2**). It describes a single phase fluid flow rate Q through a porous medium as a function of the permeability of the medium k , the cross sectional area A , the fluid's viscosity μ and the pressure gradient $\frac{\Delta p}{L}$. (Darcy, 1856)

$$Q = \frac{kA}{\mu L} \Delta p \quad \text{Eq. 2.1}$$

The formulation can be reduced to its instantaneous flux q .

$$q = \frac{Q}{A} = \frac{k}{\mu L} \Delta p \quad \text{Eq. 2.2}$$

Darcy's law is only applicable so long as the fluid flow is single phase. A two phase fluid undergoes phase segregation due to interaction of the phases with each other and with the surrounding lithology. This phenomenon can be accounted for using relative permeability (Eq. 2.3), wherein the effective permeability of a phase is dependent on the liquid saturation in the flowing fluid, and where a phase's relative permeability k_{ri} is the phase's permeability k_i over the absolute permeability k .

$$k_{ri} = \frac{k_i}{k} \quad \text{Eq. 2.3}$$

Relative permeability calculations yield a diagram called *relative permeability curves*, where the relative permeability of each phase is displayed as a function of the wetting phase saturation.

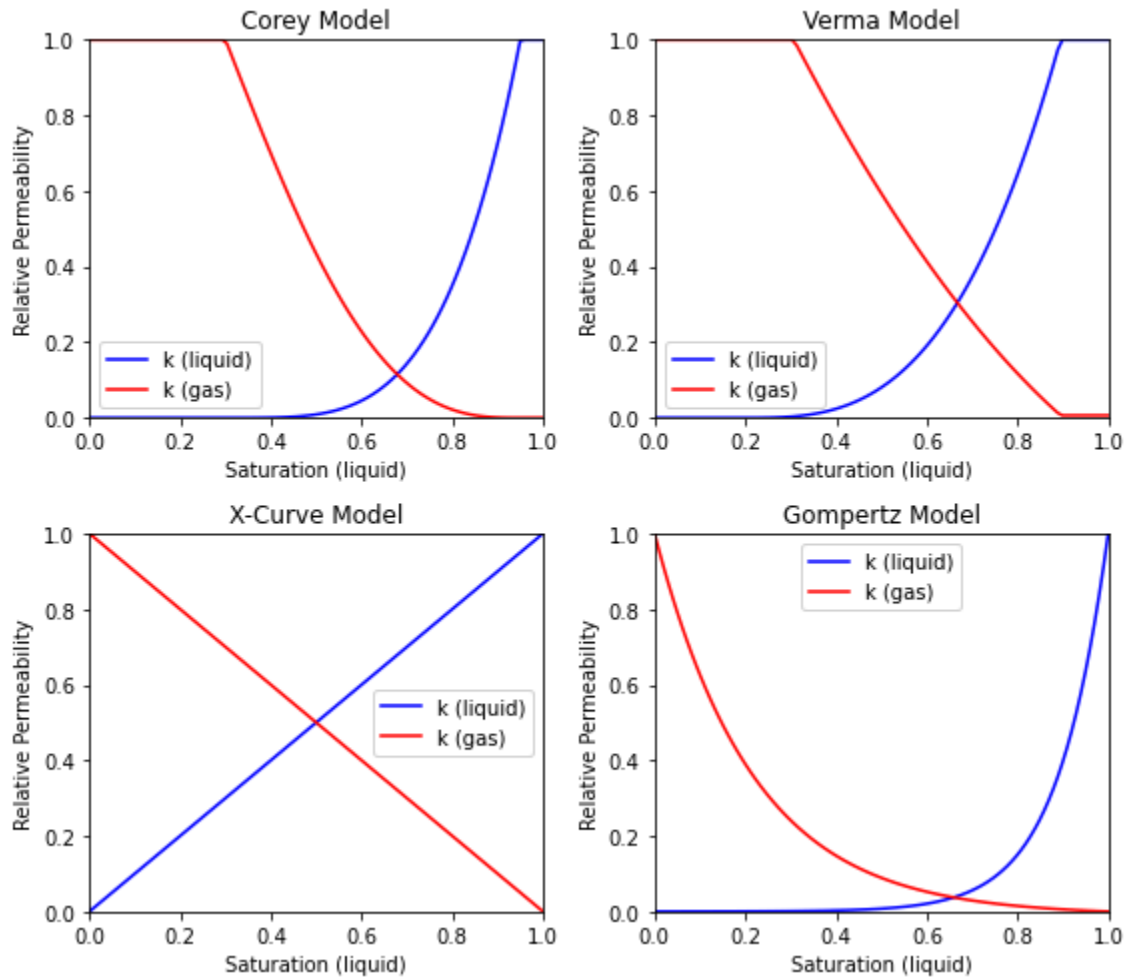


Figure 2.1 Examples of the various mathematical and empirically derived relative permeability models.

Various different models for fitting relative permeability curves to observed data exist (**Figure 2.1**) and each was developed for the needs of various applications (Corey, 1954; Verma, 1986) with the sigmoidal Gompertz growth curve proving to be adaptable to relative permeability applications. The most straightforward model is X-curves: A linear combination of the liquid and vapour phases, where it is assumed that no interaction between phases and lithology happens. That model is however not very useful for our application. Because of their high flexibility when it comes to data fitting we use Gompertz S-curves for our base case and fit the curve into a range commonly seen in comparable works (Sandström, 2021; Gudjonsdottir et al. 2015) using the values in **table 2.1**. Finally, the models use the IAPWS-IF97 formulation for the thermodynamic properties of water and steam. (IAPWS, 2007)

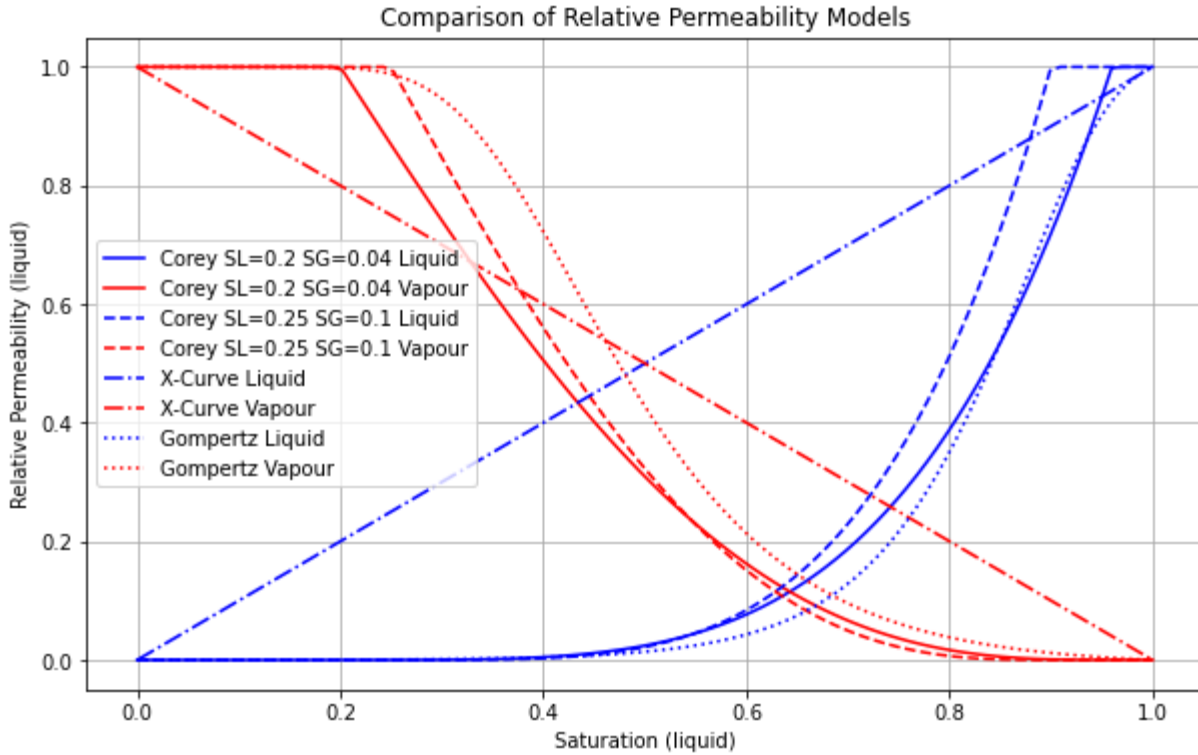


Figure 2.1 The Gompertz S-curves used for the base case model compared to a linear x-curve (no relative permeability) and the Corey curves studied in Sandström (2021).

Another layer of complexity is added to this phenomenon when one considers that the phase saturation of water, as opposed to oil and gas, also changes as it flows through the reservoir and undergoes changes in temperature and pressure. This effect makes enthalpy measurements using tracers particularly hard, as small pressure differentials can dramatically alter the dissolved tracer concentration (as discussed in section 1.1.2)

Table 2.1 The parameters of the Gompertz S-curve used to approximate a Corey (0.3, 0.05) curve. b is the x -displacement of the function and c controls the growth rate.

Parameter	Value
b (liquid)	-9.983043000
c (vapour)	-11.40507800
b (liquid)	-4.678291000
c (vapour)	-8.222140000

2.2 Model Setup

The **structural model** is set up using Brynhild's integrated tartan grid model generator. The concept is kept very simple. The model is 6x6 km long and 4.4 km deep. The grid is set to be denser towards the middle of the model's upper half to get a higher resolution around the feed zone and any occurring boiling zone.

The **lithological model** has a single porosity basement lithology below 2250 m. Above that, there is a 2250m thick MINC 3D reservoir layer. This is then topped by a 300m single porosity caprock. The reservoir layer is replaced by a permeable single porosity layer towards the edges of the model to decrease calculation intensity and to control the mode of groundwater circulation.

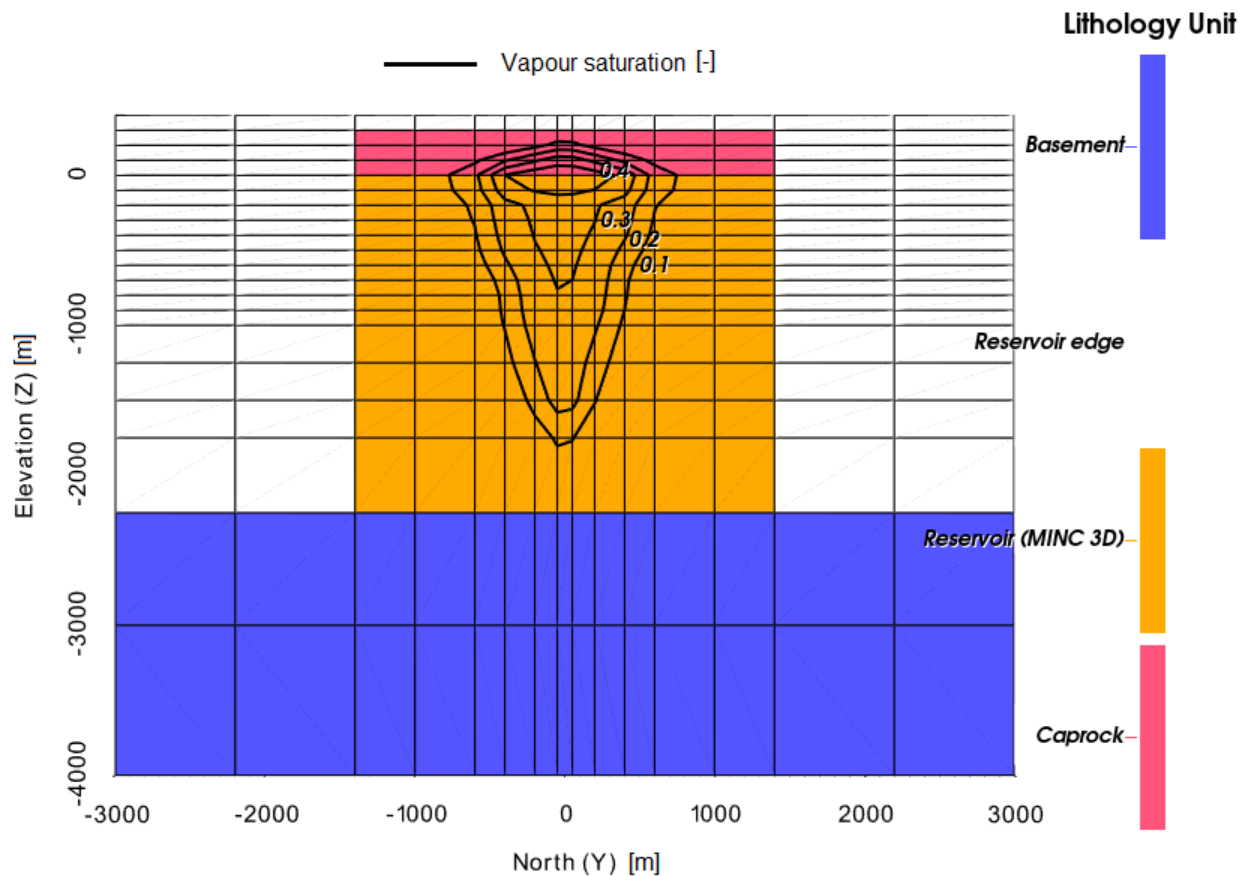


Figure 2.2: A cross section of the lithological model with the boiling cap from the boiling reservoir superimposed in the form of vapour saturation isolines. It is composed of four lithologies and has a higher discretization density towards the top of the reservoir to address boiling cap formation. The lithological properties are listed in table 2.2.

The model is topped with an atmosphere block that facilitates cooling through atmospheric interaction set to 15°C at 101325 Pa. The bottom layer of the model introduces 0.15 W m⁻² of conductive heating. This is somewhat higher than average oceanic lithosphere at 0.1 W m⁻² (Pollack et al. 1993) but eminently reasonable for a more geothermally active area where higher

than average heat flow occurs. To further justify this value one can consider a temperature gradient of $200 \text{ }^\circ\text{C km}^{-1}$ with a typical thermal conductivity of $2 \text{ W m}^{-1} \text{ K}^{-1}$ (Hayba and Ingebritsen 1994), which results in a surface heat flux of 0.4 W m^{-2} . Geothermal heat flow in geothermal areas is usually convectively dominated and makes conductive heat flow in such areas hard to quantify (Pollack et al. 1993; Stein and Stein 1992). Since conductive heat flux in the ocean crust relates to its age but becomes unreliable in younger, more permeable regions, we stick to that conservative estimation of 0.15 W m^{-2} . This bottom layer heat flux is already enough to initiate weak groundwater convection before introducing the convective heat source.

The system's convective heat source is placed in a 5×5 cell grid in the bottom layer of the model and has an area of 640000 m^2 . The heat source comes in two variants to produce either a boiling system or a sub-boiling system. The boiling aquifer is fed with 20 kg s^{-1} of 2 MJ kg^{-1} pure water. While the sub-boiling one is fed 10 kg s^{-1} . This comes out as roughly 5 W m^{-2} and 2.5 W m^{-2} respectively above the convective zone or 62.5 W m^{-2} and 31.25 W m^{-2} in the emplacement cells. Near surface heat flux for geothermal and volcanic systems varies drastically but typically falls in the range of 10 's W m^{-2} . (Wang and Pang 2022)

For our base case we consider a fracture dominated network in a fractured igneous rock with a typical fracture permeability value of $1 \text{e}^{-14} \text{ m}^2$ (Schön, 2015). The matrix permeability is set to 1e^{-16} (Johnson, 2006), and fracture spacing is kept at 100 m equidistant for x , y and z to have at least one set of fractures in each representative elementary volume. Previous works place the fracture spacing in the range of $150\text{-}250\text{m}$ (Ratouis et al. 2019, Ratouis et al. 2022, Gebru 2023) but we will assume a highly fractured reservoir and compare it to a range including these values in section 3.3.3. A feed zone at -850 m_z elevation (or 1250 m downhole) feeds fluid into the production well, this will place it in the centre of the reservoir lithology, and in case of the boiling aquifer it is just below the centre of the boiling cap. Finally, in the Hellisheiði and Hengill geothermal fields, feed zones used for production can be found in a wide range of depths from a few hundred metres to over two kilometres with many existing around $1000\text{-}1500 \text{ m}$ depth (Björnsson, 2004; Poux et al. 2021).

Table 2.2: *The reservoir properties of the base case model. The increased complexity of the MINC model is apparent over the single porosity models when one considers the amount of parameters at play.*

	Reservoir	Edges	Caprock	Basement
Porosity, matrix (fracture) [-]	0.1(0.9)	0.15	0.05	0.1
Permeability¹ [m^2]	-	1e^{-14}	1e^{-16}	1e^{-15}
Fracture permeability [m^2]	1e^{-14}	-	-	-
Matrix permeability [m^2]	1e^{-16}	-	-	-
Fracture spacing² [m]	100	-	-	-
Feed zone depth³ [m]	-850	-	-	-

Matrix volume fraction [-]	0.85	-	-	-
Rock density [kg m⁻³]	2800	2800	2800	2800
Specific heat [J kg⁻¹ K⁻¹]	1200	1200	1200	1200
Heat Conductivity [W m⁻¹ K⁻¹]	2	2	2	2
Relative permeability	Gompertz S-curves (table 2.1)			

1. In single porosity lithologies
2. Isometrically for all three fracture planes of the model.
3. From the z axis origin. The model surface is 400m above the origin, placing it 1250 m downhole.

2.3 Natural state

The natural state models were created to represent two reservoir types. Each model is allowed 3.6m years to reach its natural state in two iterations. First the bottom heat conduction is allowed to reach equilibrium with the atmosphere. That iteration is then overprinted by introducing the upwelling zone and allowing it to reach equilibrium.

2.4 Simulation approach

The simulations are conducted from the natural state by introducing a production well and then running the model to simulate two decades of production. After exporting the production data, the parameters are changed and new production data is made.

The production well has a lining with an ID of 17.78 cm (7") and an OD of 30 cm (11.81"). This is an intermediate size between the typical sizes used as high temperature geothermal casings (Þórhallsson, 2003) with a feed zone at 1100m downhole. The production stage is set to run for 20 years. The well is given a feed zone with a very high permeability of 1e-12 m². This ensures that the feed zone is not the bottleneck and thus masking the reservoir behaviour. The feed zone is always appended to the middle of its respective elementary volume. The wellhead pressure is set to be constant at 10 MPa. (Grant and Bixley, 2011)

The procedure of exploring the parameters influencing EEDs involves primarily altering fracture permeability, matrix permeability, fracture spacing, feed zone depth and relative permeability curves, and in some cases a combination of these parameters.

3. Results

In this chapter the results of every simulation will be presented, starting with the natural state simulations (section 3.1), followed by looking into the base case of production (section 3.2) before looking into the sensitivity analysis of the various parameters (section 3.3) and the effect of production on reservoir conditions (section 3.4).

3.1 Natural state

The boiling aquifer (Fig. 3.1.1) developed a boiling zone extending 1800m vertically with a boiling cap, 1200m a side. It reached vapour saturation of over 0.5 in the central boiling cap. The boiling aquifers had a reservoir temperature ranging from 273°C to 373°C along the welltrack and the sub-boiling aquifers had a reservoir temperature ranging from 268°C to 319°C along the welltrack (figure 3.1.2).

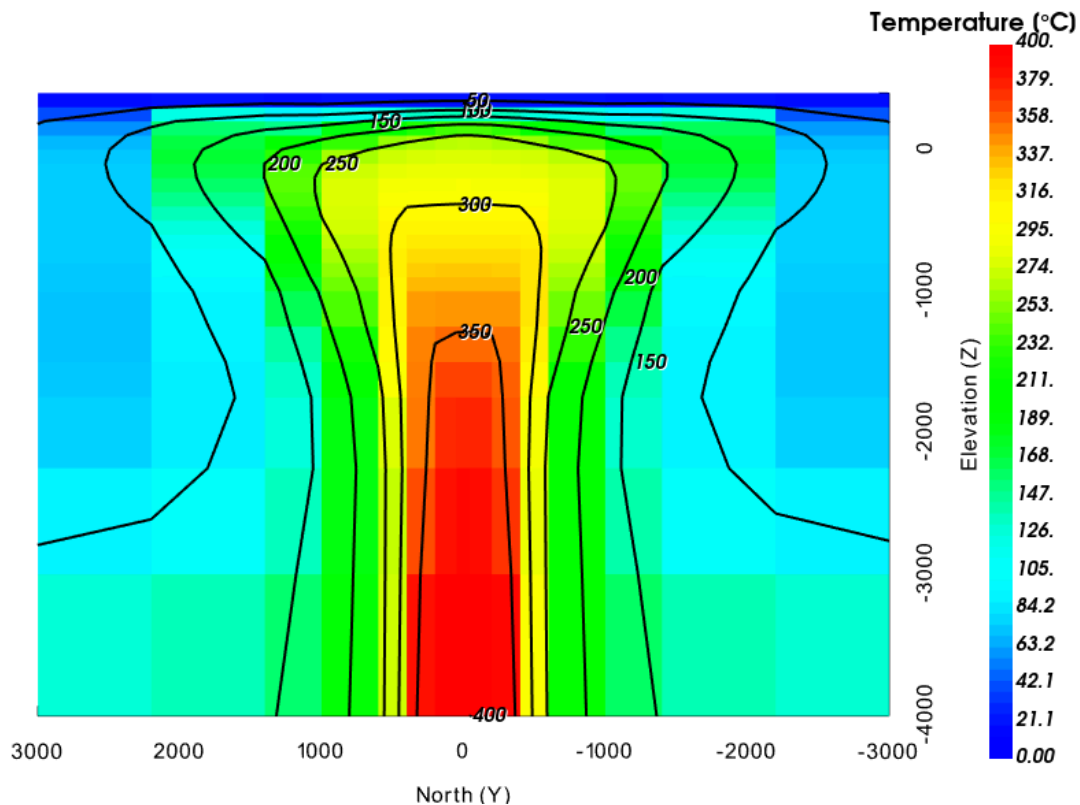


Figure 3.1.1 A north-south cross section of the boiling model.

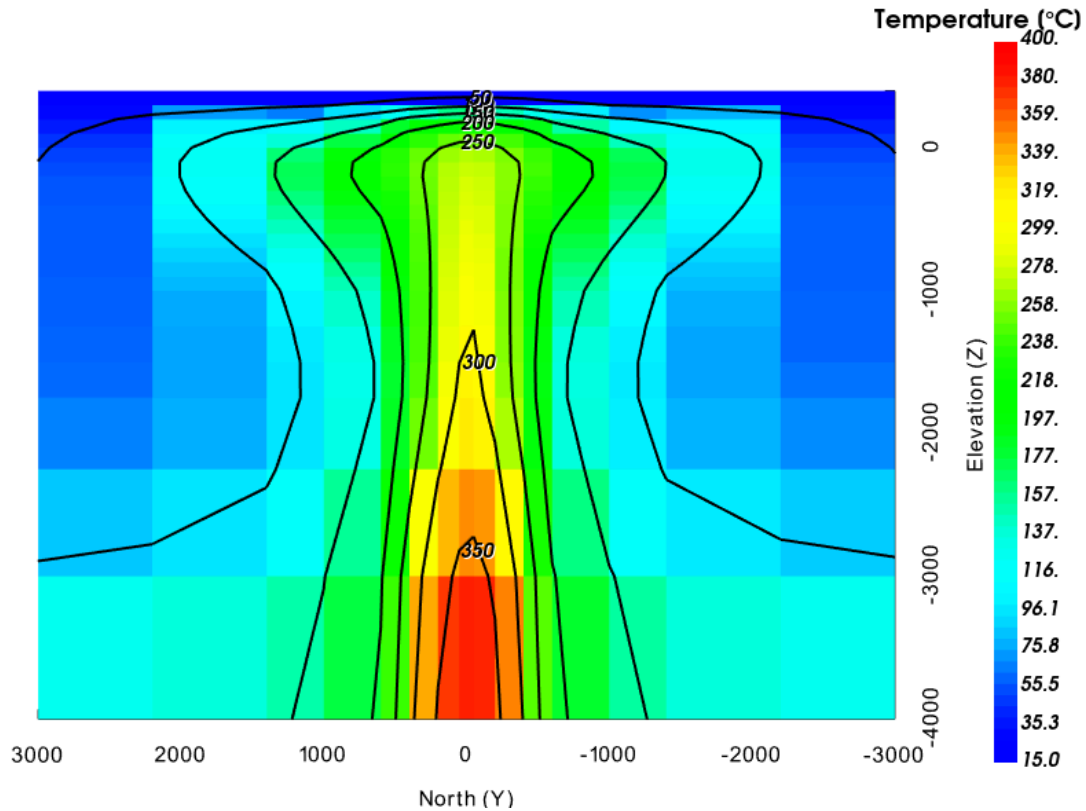


Figure 3.1.2 A north-south cross section of the sub-boiling model.

3.2 Base case

From the plot in **Figure 3.2.1** we see excess enthalpy developing in the boiling reservoir. After an initial spike in enthalpy there is a smooth increase peaking around four years into production before slowly dipping below the initial discharge enthalpy. This results from the decompression boiling in the reservoir as the pressure controlling phase (vapour) gets pumped out. The initial spike in vapour is only present in the cell hosting the feed zone while the slow increase follows the transient pressure change as it invades a larger volume, until the recharge plume below starts drawing in colder fluids from the edge of the reservoir. Put simply, for our base case we see an EED in boiling reservoirs and none in sub-boiling reservoirs.

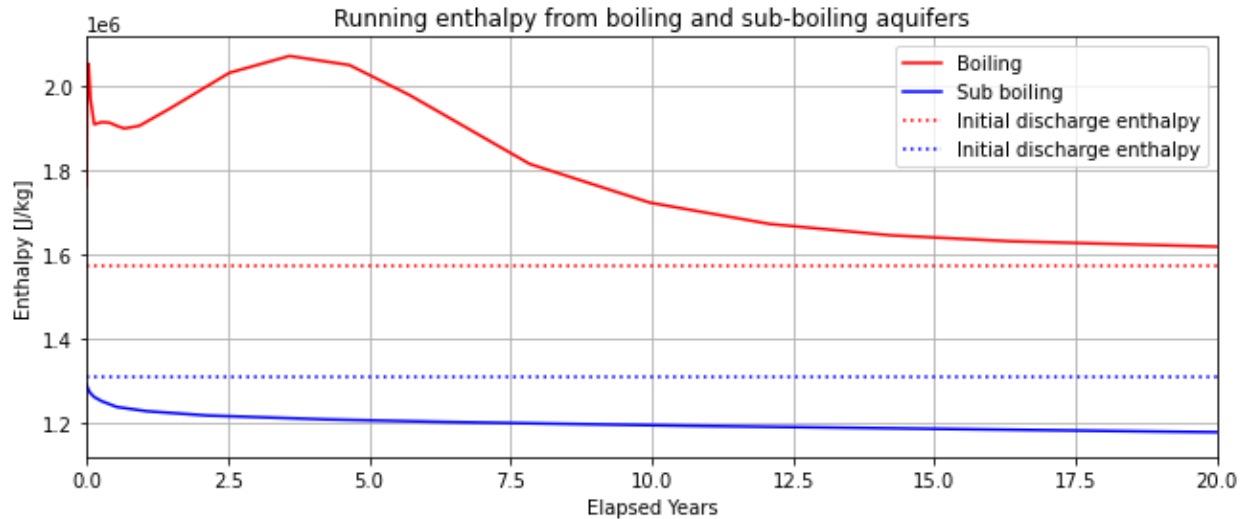


Figure 3.2.1 The running enthalpy of the base cases for each reservoir type. In the boiling reservoir we see excess enthalpy developing in the first years of production before slowly approaching but not matching, the initial reservoir enthalpy.

3.3 Controls on well discharge enthalpy

To elucidate exactly which factors control the onset of excess enthalpy discharges and to what extent they do so, we perform sensitivity analysis on groups of production datasets in which only one parameter is adjusted. Gas mass fraction and enthalpy are intrinsically related and will graph identically when scaled to their respective measurement units on a running enthalpy diagram. Capping out at around 2200-2800 kJ/kg for saturated vapour (**Figure 1.1**) Meaning that for a saturated vapour the control for enthalpy is pressure. In our case we chose a wellhead pressure of 1 MPa (**Section 2.2.**) Pre-existing vapour in the aquifer will almost always induce EEDs due to flashing at the start of production with additional EED as the pressure drop invades the surrounding lithology and induces more boiling. Furthermore, producing from a boiling cap plays a big role as seen in the base case (**section 3.2**).

3.3.1 Fracture permeability

Sensitivity analysis of fracture permeability in both boiling and sub-boiling models indicate that fracture permeability has a strong influence on the occurrence and the type of excess enthalpy discharges. The boiling aquifer has a high tendency for EEDs even under high permeabilities due to the amount of pre-existing vapour present in the system. The onset of enthalpy fluctuation due to phase segregation is between $5e-15$ m² and $2e-15$ m² and is characterised by large, short lived spikes in enthalpy, followed by deeper recessions. (**Fig. 3.3.1**) The sub-boiling aquifer shows no EEDs unless the fracture permeability is very low, in which case it displays sharp spikes followed by a period of recovery (**Fig. 3.3.2**). These spikes also have some periodicity to them and are accompanied by flashing in the feed-zone hosting cell. The periodicity likely stems from the symmetry and uniformity of our simple model, along with the low permeability not enabling sufficient recharge to continue the flashing process, and the fact that

the aquifer is not overheated enough to cause outwardly cascading flash boiling that would introduce a more chaotic pattern like we see in the boiling aquifer. Perhaps unsurprisingly, the rate of enthalpy decrease is faster in more permeable systems. The conclusion is that lower fracture permeabilities tend to incite phase segregation and sporadic EEDs, while high enough permeabilities can reduce EEDs through a more rapid inflow of cold water from the sides.

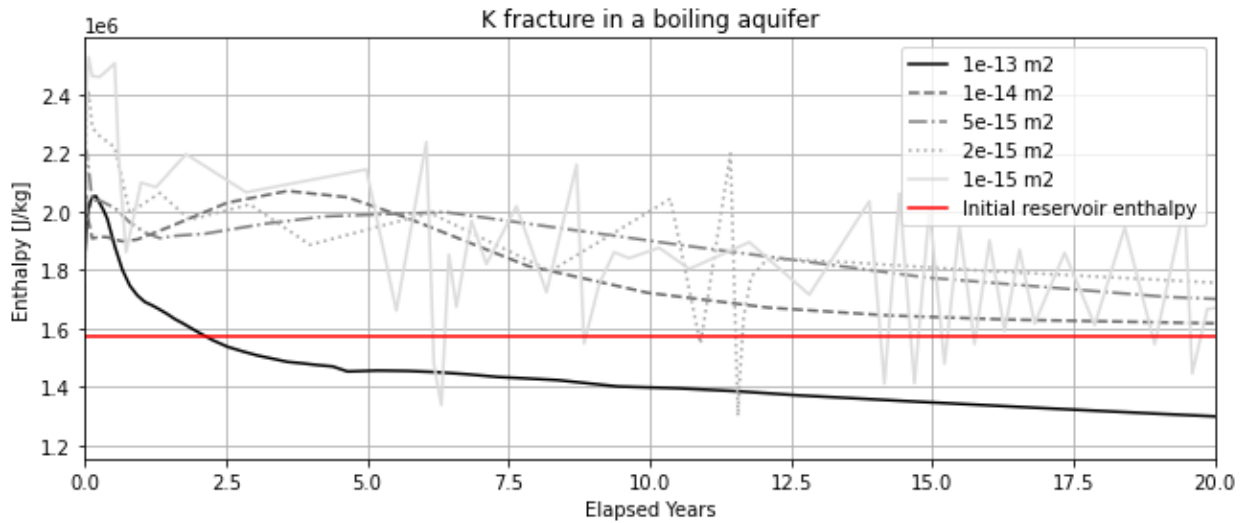


Figure 3.3.1. The running enthalpy of varying fracture permeabilities in a boiling aquifer. Every permeability starts with some initial excess enthalpy. The leakier fractures develop toward lower enthalpies faster than tighter fractures.

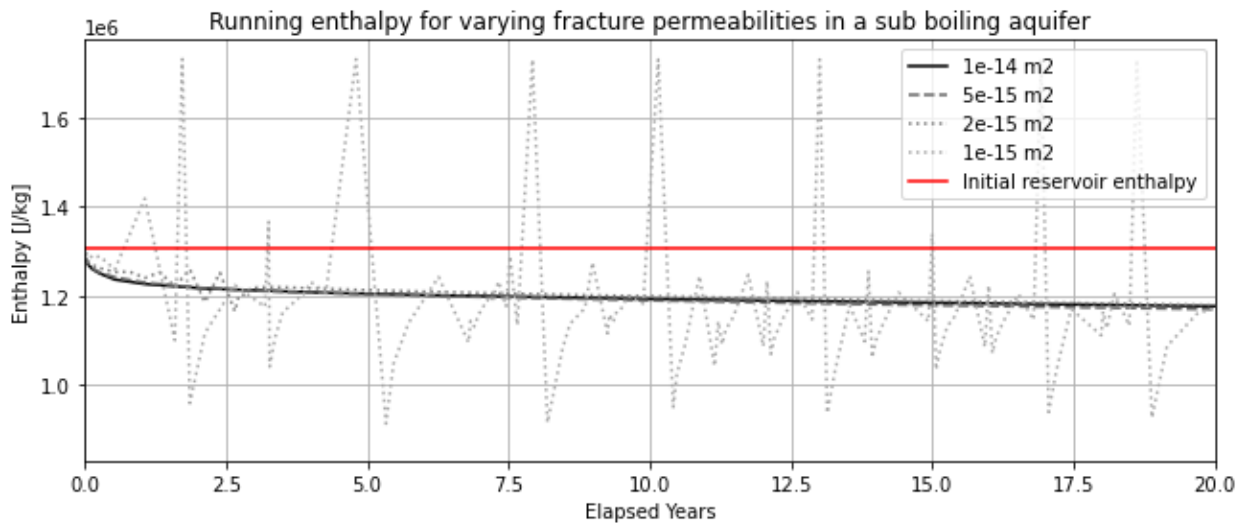


Figure 3.3.2. The running enthalpy of varying fracture permeabilities in a sub boiling aquifer. The leakier fractures quickly flatline below the IRE and vary little over time. Tightening the fractures induces EEDs.

3.3.2 Matrix permeability

Sensitivity analysis of matrix permeability shows little in terms of controlling the occurrence of EEDs. In the sub-boiling aquifer it has absolutely no influence on the running enthalpy discharge

curve (Fig. 3.3.4) The boiling aquifer enthalpy peaks at the beginning and quickly recedes before slowly rising again three to four years into production, after which it slowly changes into a wetter phase mixture. (Fig. 3.3.3) In a more matrix dominated lithology, the boiling aquifer stays in excess enthalpy almost the entire time, only dipping below the initial reservoir enthalpy value during periods where it rapidly changes (Fig 3.3.5)

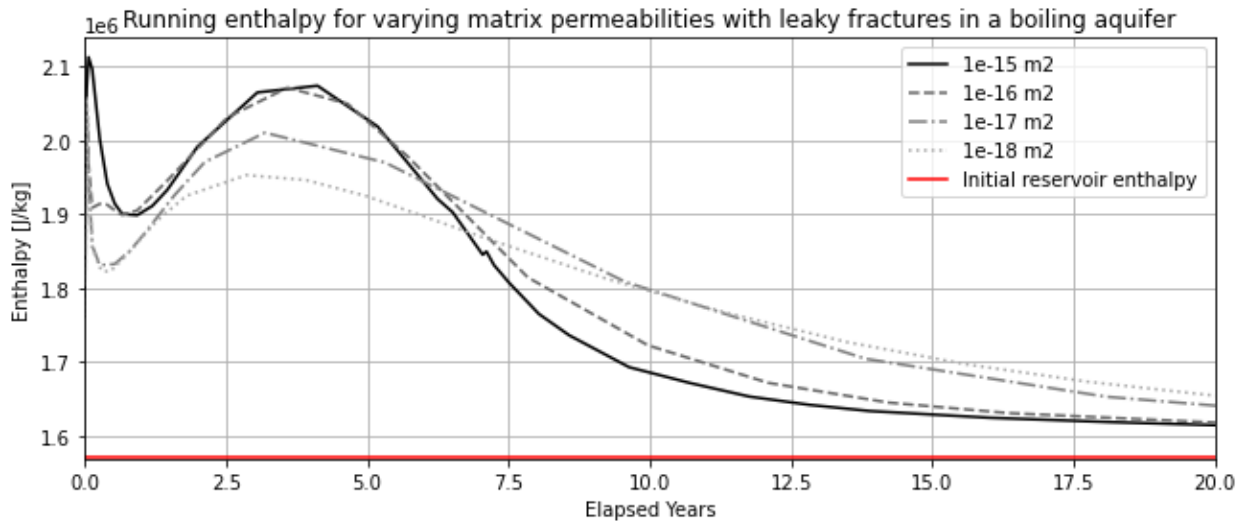


Figure 3.3.3. The running enthalpy for varying matrix permeabilities with leaky fractures in a boiling aquifer. Due to depressurisation boiling there are two peaks in production. One from the initial steam flashing around the feed zone. Another from the transient pressure change in the entire reservoir.

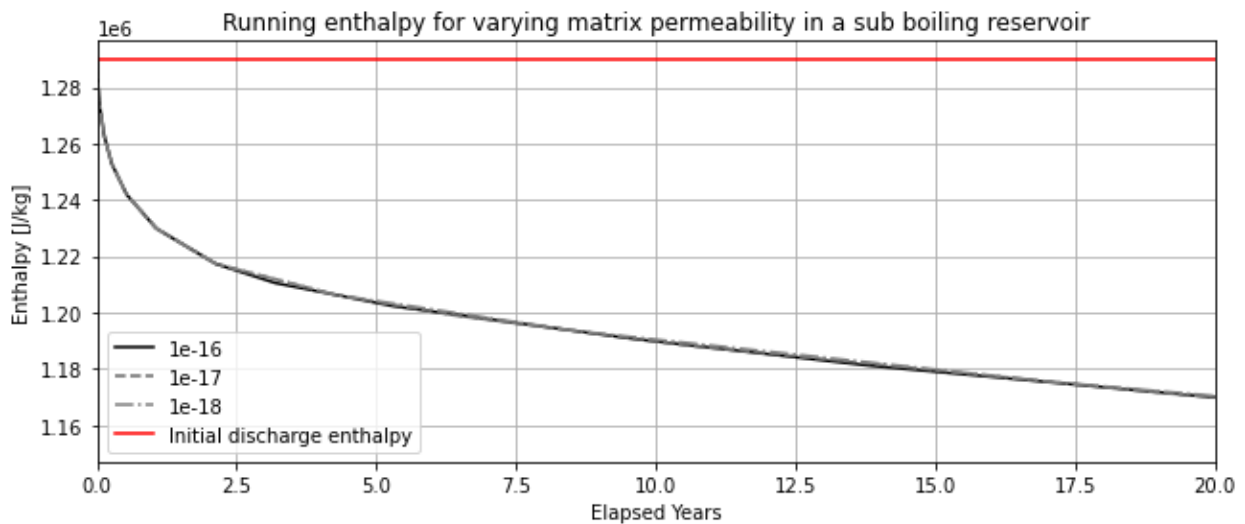


Figure 3.3.4. The running enthalpy for varying matrix permeability with leaky fractures in a sub boiling reservoir. Under these conditions the matrix permeability has practically no effect.

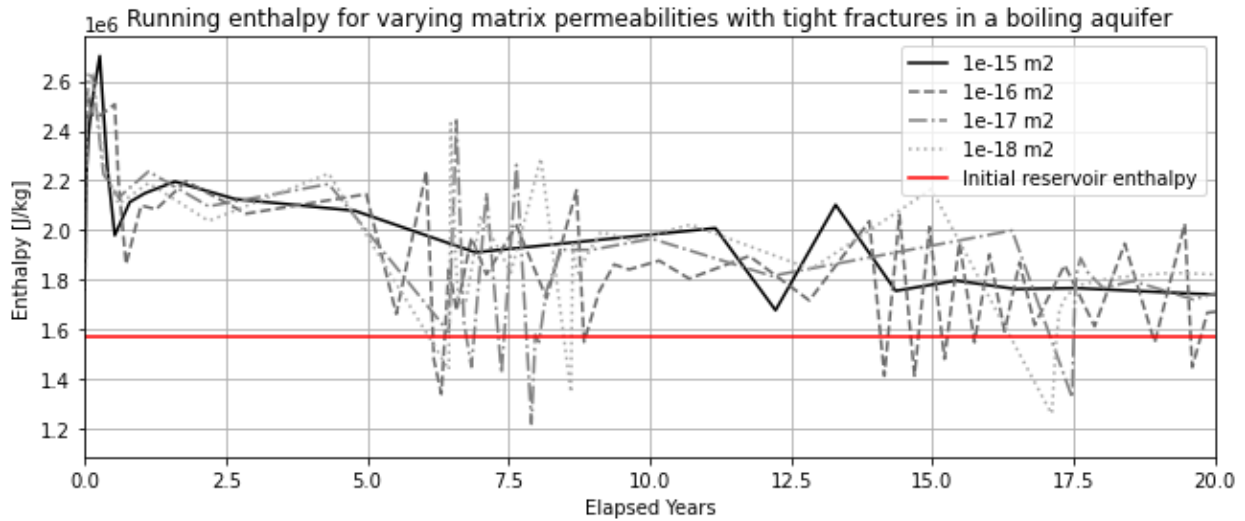


Figure 3.3.5. The running enthalpy for varying matrix permeabilities with tight fractures in a boiling aquifer. At $1e^{-15} \text{ m}^2$ the permeability contrast between matrix and fractures is none.

3.3.3 Fracture spacing

Fracture spacing has little to moderate influence on the enthalpy curves. In more permeable fracture systems, fracture spacing only slightly shifts the running enthalpy curve. The development of steam through induced boiling is slightly increased with closer fractures. (**Fig 3.3.6**) For tighter formations a smaller spacing tends to smooth out the rapid discharges (**Figs. 3.3.7 and 3.3.8**) as a denser network of fractures has an easier time equilibrating whatever segregation occurs in it, i.e. more fractures per REV leaves less chance for a single fracture being dominantly representative, just like a leakier matrix may smooth out any stronger variations in fractures.

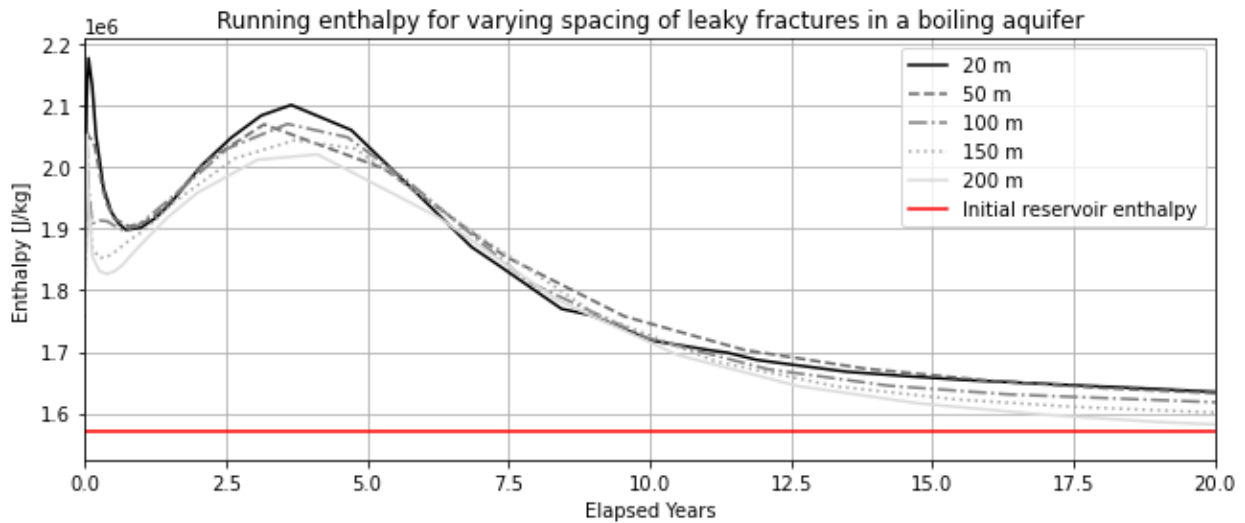


Figure 3.3.6. The running enthalpy for varying fracture spacing of leaky fractures in a boiling aquifer. These variations have a similar but smaller effect to varying the matrix permeability.

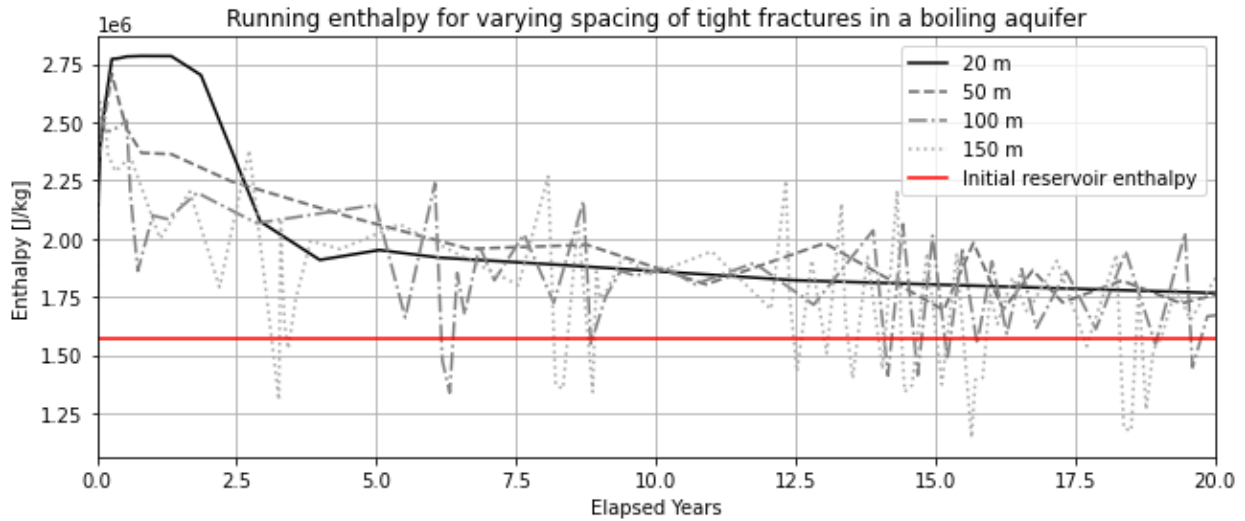


Figure 3.3.7 The running enthalpy for varying spacing of tight fractures in a boiling aquifer. Tightening the fracture spacing smooths out the EEDs similar to having high matrix permeability.

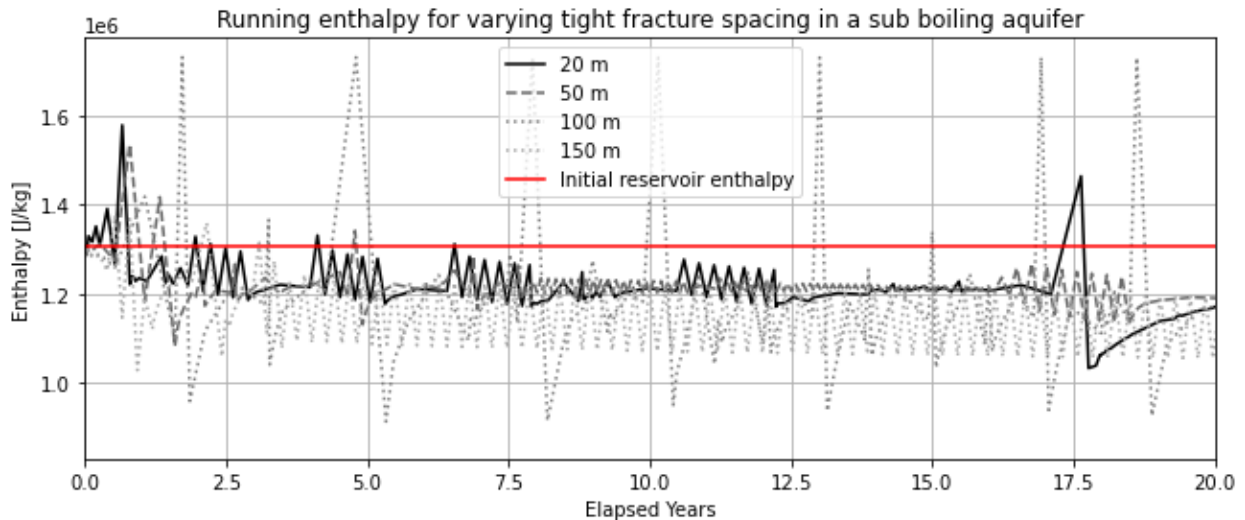


Figure 3.3.8 The running enthalpy for varying spacing of tight fractures in a sub boiling aquifer. Tightening the fracture spacing smooths out the EEDs like in the example above. Depressurisation induces some flashing. Tight spacing seems to somewhat level out the magnitude of the fluctuations and introduce longer rest periods.

3.3.4 Depth of feed zone

The depth of the feed zone has an intermediate to strong effect on the enthalpy curve (**Figs. 3.3.9 -3.3.11**). Feed zone depth can temporally shift induced boiling curves. Another effect to consider is the contrast of reservoir and wellhead pressure. The wellhead pressure was kept constant while fluid flow from the reservoir came in at varying pressures. This may also affect fluid behaviour along the well track while being delivered to the surface as the well pressure gradient may vary. The IRE is different for the various feed zones and the amplitude of excess enthalpy grows relative to IRE with shallower depth as the feed zone has access to more

recharge from the boiling cap below (See figures 3.4.2 & 3.4.3). Feed zone depth has no effect on enthalpy discharge from sub-boiling aquifers (fig. 3.3.12).

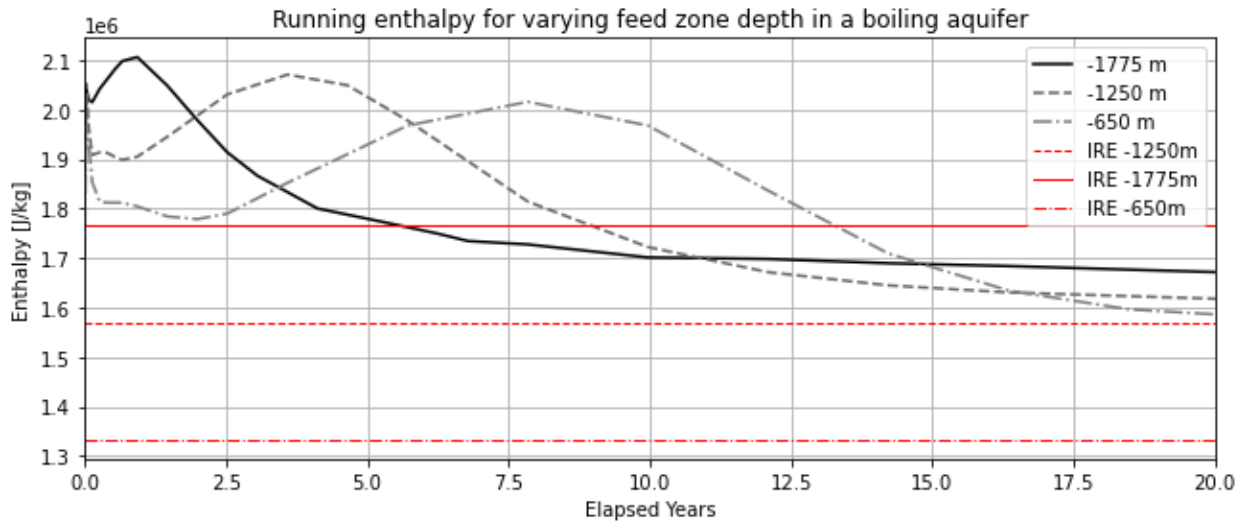


Figure 3.3.9. The running enthalpy for varying feed zone depth in a leaky boiling aquifer. Shallower feed zones have access to a greater amount of vapour recharge from below, leading to a temporal elongation of the induced boiling in the aquifer. The IRE of each scenario is different since enthalpy can vary by elementary model volumes.

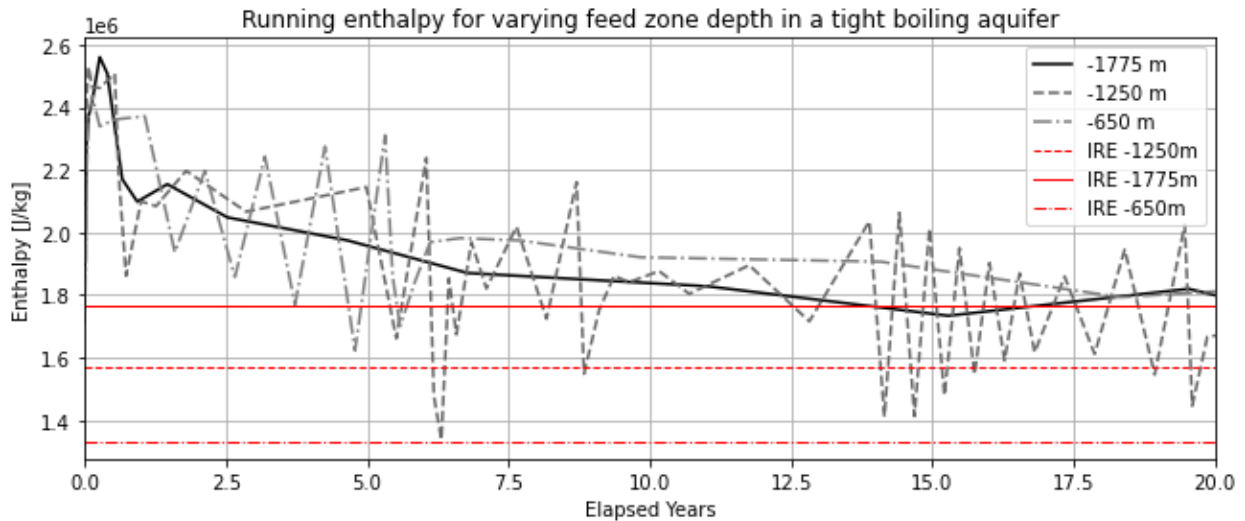


Figure 3.3.10. The running enthalpy for varying feed zone depth in a tight boiling aquifer. The shallow feed zone stays well in the EED region for the entire runtime due to access to vapour recharge from below.

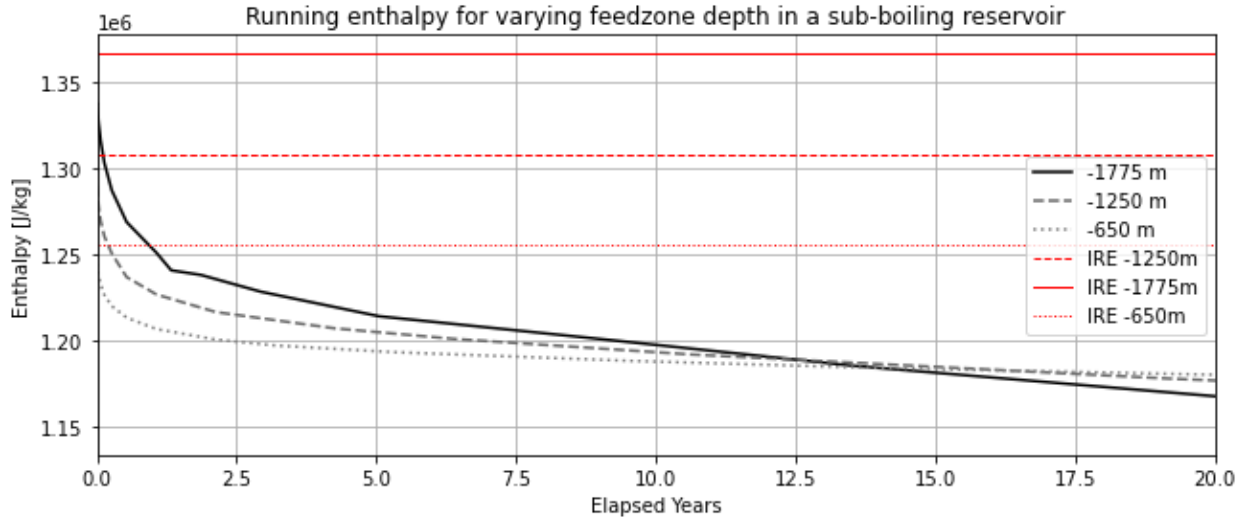


Figure 3.3.11. The running enthalpy for varying feed zone depth in a leaky sub-boiling reservoir. Varying the feed zone depth seems to pivot the enthalpy curve, but as in other high permeability/ sub-boiling reservoirs, there is no EED.

3.3.5 Matrix volume fraction

The matrix volume fraction controls the elongation of the induced boiling curve of the high fracture permeability aquifer (**Fig. 3.3.12**) and accelerates the drop in enthalpy when set to high values (**Figs. 3.3.12 & 3.3.13**). The tighter aquifer sees the parameter affect the frequency of enthalpy spikes with lower values decreasing their frequency and amplitude while introducing slower recovery curves (**fig. 3.3.14**).

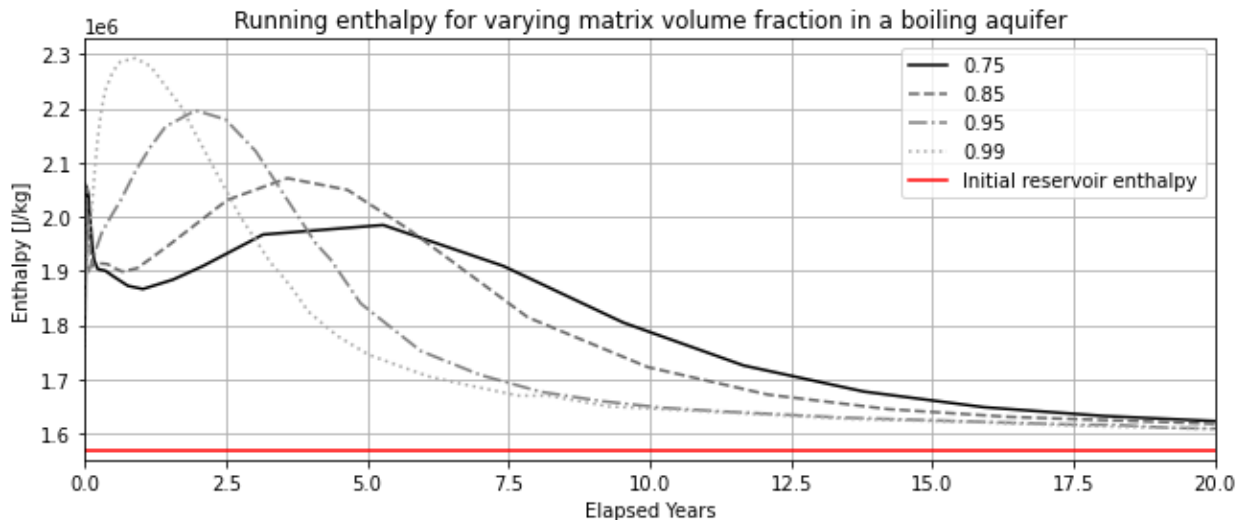


Figure 3.3.12 The running enthalpy for varying matrix volume fraction in a boiling aquifer. Higher matrix fractions cause more discharge early as opposed to a smaller increase over a longer time with a delayed onset.

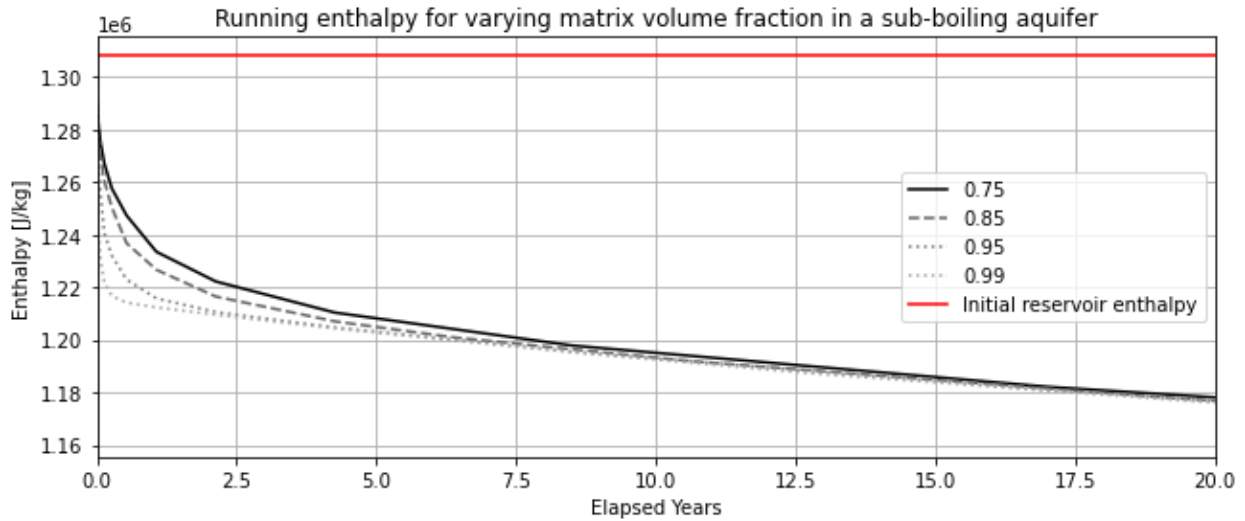


Figure 3.3.13. The running enthalpy for varying matrix volume fraction in a leaky, sub-boiling aquifer. Higher values increase the rate of initial enthalpy decrease.

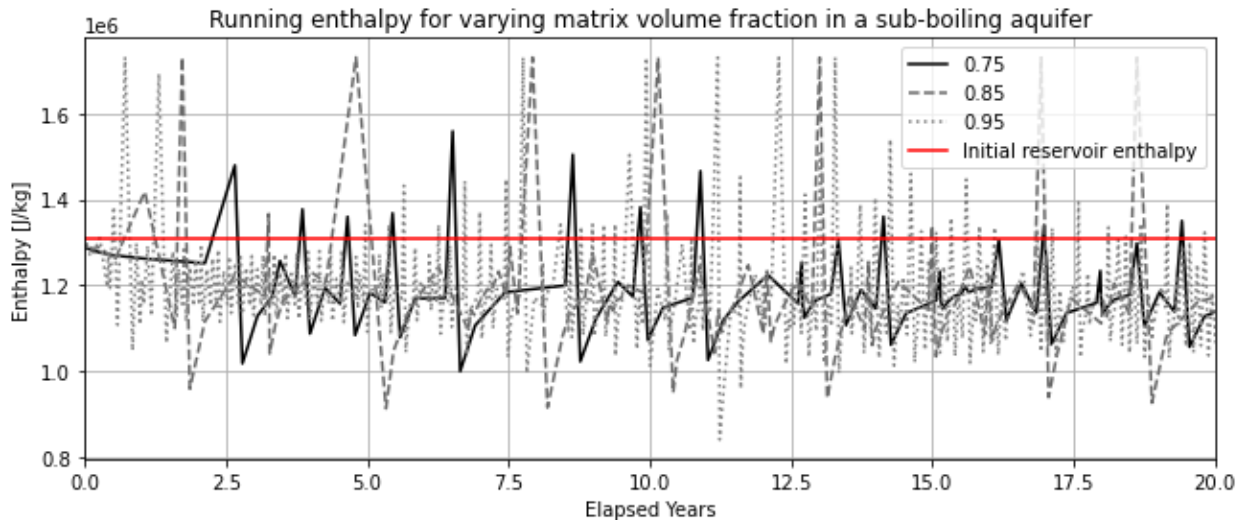


Figure 3.3.14. The running enthalpy for varying matrix permeability in a tight, sub-boiling aquifer. Higher values increase the frequency and amplitude of enthalpy spiking.

3.3.6 Relative permeability curves

The influence of relative permeability models on the development of EEDs was covered by Sandström (2021) where it was found that enthalpy and pressure evolution using x-curves were not sufficient to reach the higher flowing enthalpy values achieved by Corey curves ($<1700 \text{ kJ kg}^{-1}$ and $<2200 \text{ kJ kg}^{-1}$ respectively). In **fig. 2.1** we compare those curves to our base case Gompertz curve. The resulting flowing enthalpy curves are plotted in **fig 3.3.15**. Relative permeability curves dictate how effectively each phase flows in the presence of the other. It is therefore unsurprising to see that there is a significant difference in the flowing enthalpy curves, with higher liquid saturation values promoting higher running enthalpy. However, even linear relative permeability flow exceeds the IRE for around eight years due to depressurisation

boiling. In a sub-boiling low fracture permeability reservoir, altering the relative permeability curves has a significant effect on the occurrence of EEDs (**fig. 3.3.16**). In conclusion, depending on the mode of the EEDs relative permeability curves have either an intermediate or strong influence.

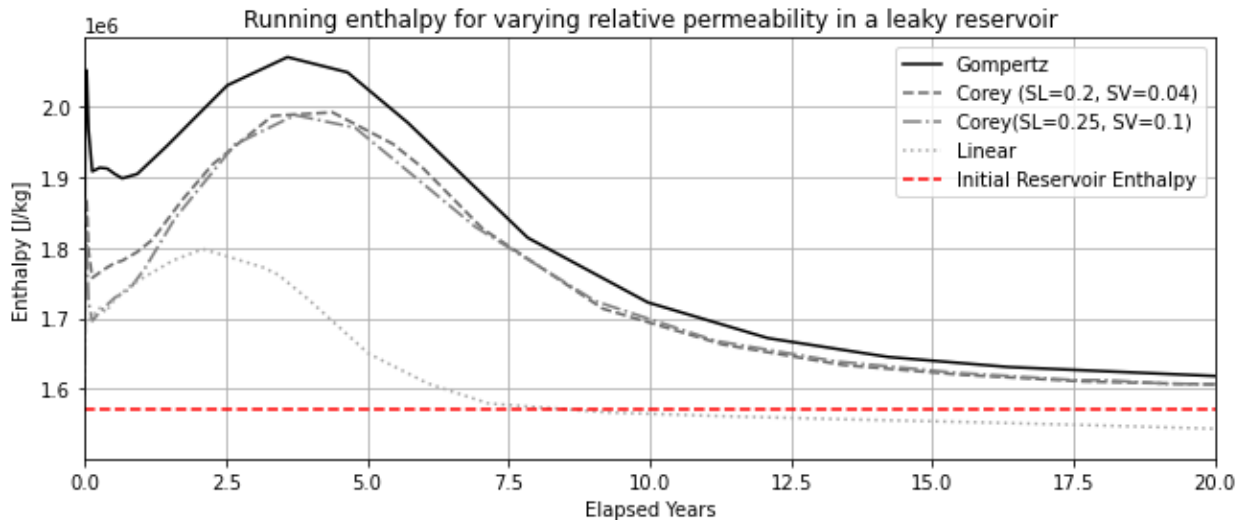


Figure 3.3.15. The running enthalpy for varying relative permeability curves in a boiling high permeability reservoir. The Gompertz curve is roughly equivalent to a $SL=0.3$ $SV=0.05$ Corey curve.

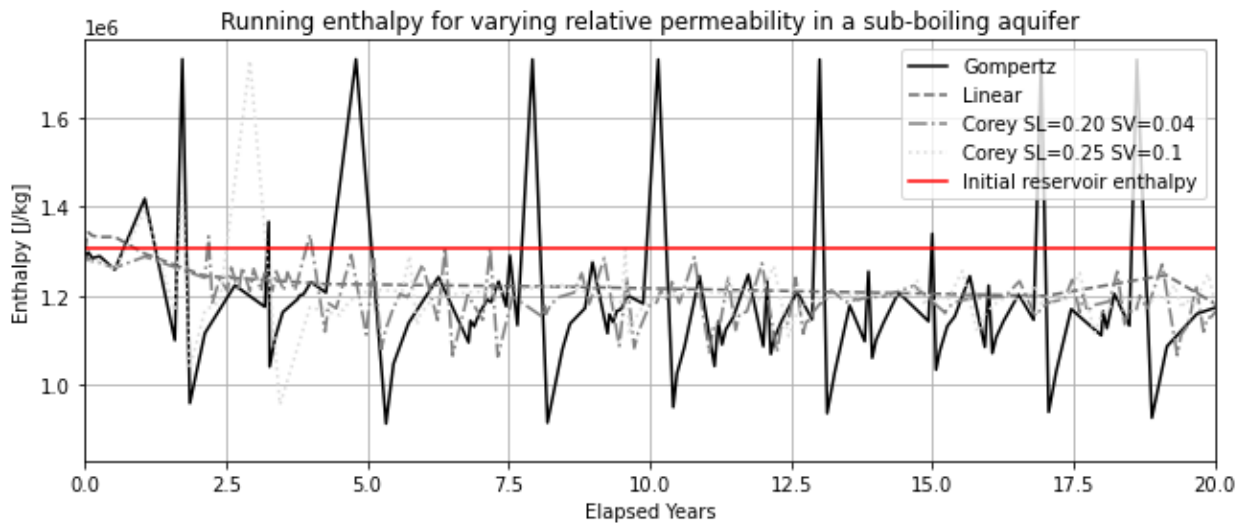


Figure 3.3.16. The running enthalpy for varying relative permeability curves in a sub-boiling low permeability aquifer. The dominant mode of EEDs is flashing in the feed zone hosting cell. The Gompertz model is roughly equivalent to a Corey $SL=0.3$ $SV=0.05$ curve.

3.4 Impact of production on reservoir

Production inevitably will affect the reservoir around it. In both models and under most parameter variations there was an increase in boiling. The liquid dominated reservoir exhibited semi regular flash boiling in the feed zone cell under low fracture permeability and in any case

had a small steam cap forming after only a few months to years (**fig. 3.4.4**). Pressure drawdown travels extensively downwards and outwards into the reservoir basement (**figs. 3.4.3 & 3.4.4**) The sub-boiling reservoir also sees a lower pressure in the upper plume, apart from the small boiling cap, where induced boiling actually increases the pressure slightly. In the boiling reservoir the additional boiling raises the pressure in the plume head significantly, by up to 0.775 MPa. The pressure drawdown is accompanied by a temperature drop of up to 20°C below the feed zone and a temperature rise of 4 °C in the plume head (**fig. 3.4.5**).

The deliverability of the various models is highly variable and is controlled by the pressure gradient from bottom hole to wellhead and the phase mixture. In terms of mass rate, vapour-rich flows are smaller due to their low density. A comparison of the base cases reveals a deliverability difference of 45 kg/s between the boiling and sub-boiling reservoirs (**fig. 3.4.1**).

The deliverability curves for some models cap out at under 5 kg s⁻¹ due to the reservoir being too tight to deliver the already low density vapour any faster (**fig. 3.4.2**)

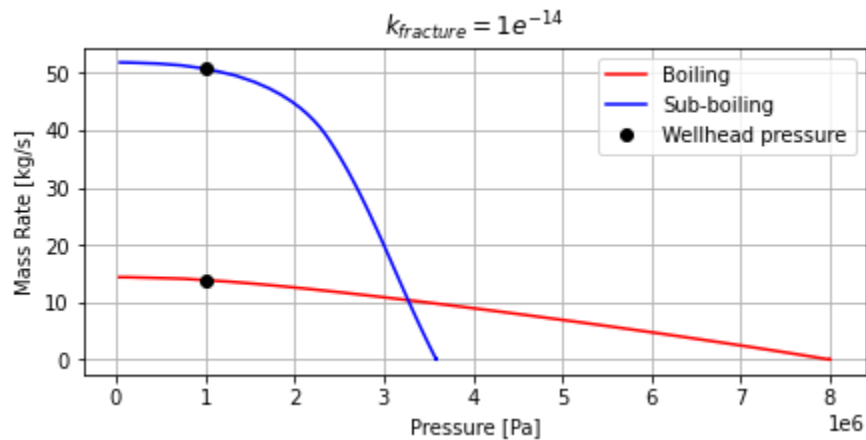


Figure 3.4.1. The deliverability curves of the base case for identical wells in identical lithologies, producing from the same depth. The boiling reservoir produces a flatter curve due to higher BHP and due to the low density of vapour.

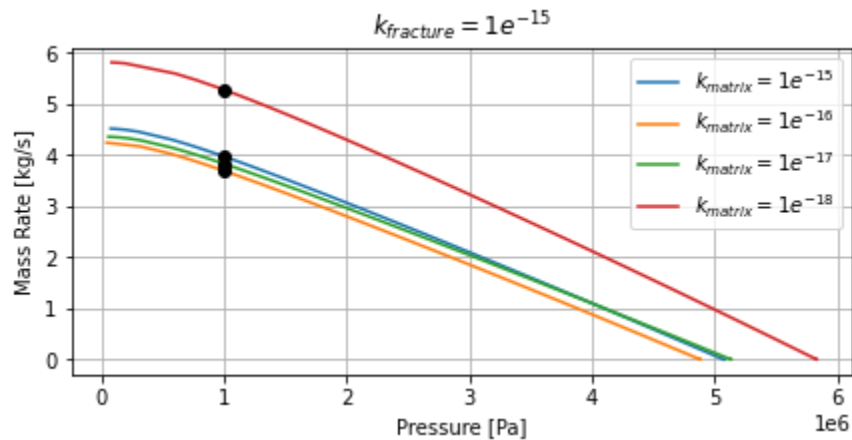


Figure 3.4.2. The deliverability curves for the models in **fig. 3.3.5** are set in a boiling aquifer with low fracture permeability.

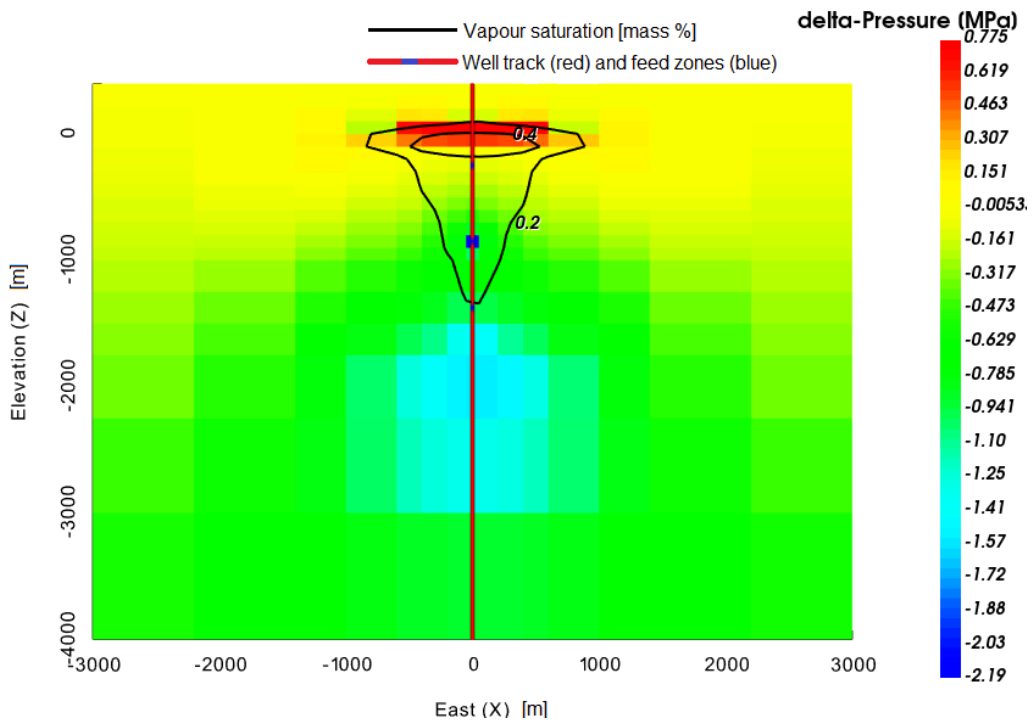


Figure 3.4.3. The pressure changes in the boiling reservoir as a result of 20 years of production in the base case (section 3.2) with superimposed vapour mass saturation isolines showing the location of the boiling cap. The blue sections on the well track represent the variations on feed zone depth analysed in section 3.3.4.

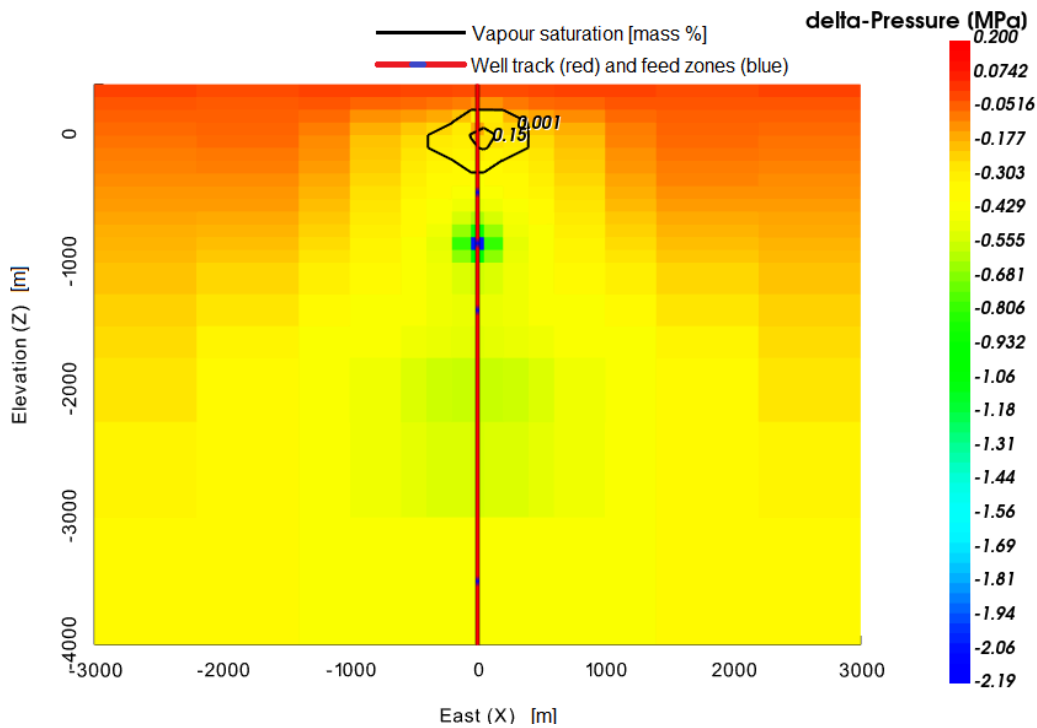


Figure 3.4.4. The pressure changes in the sub-boiling reservoir as a result of 20 years of production in the base case (section 3.2) with superimposed vapour mass saturation isolines showing the induced boiling cap as a result of production.

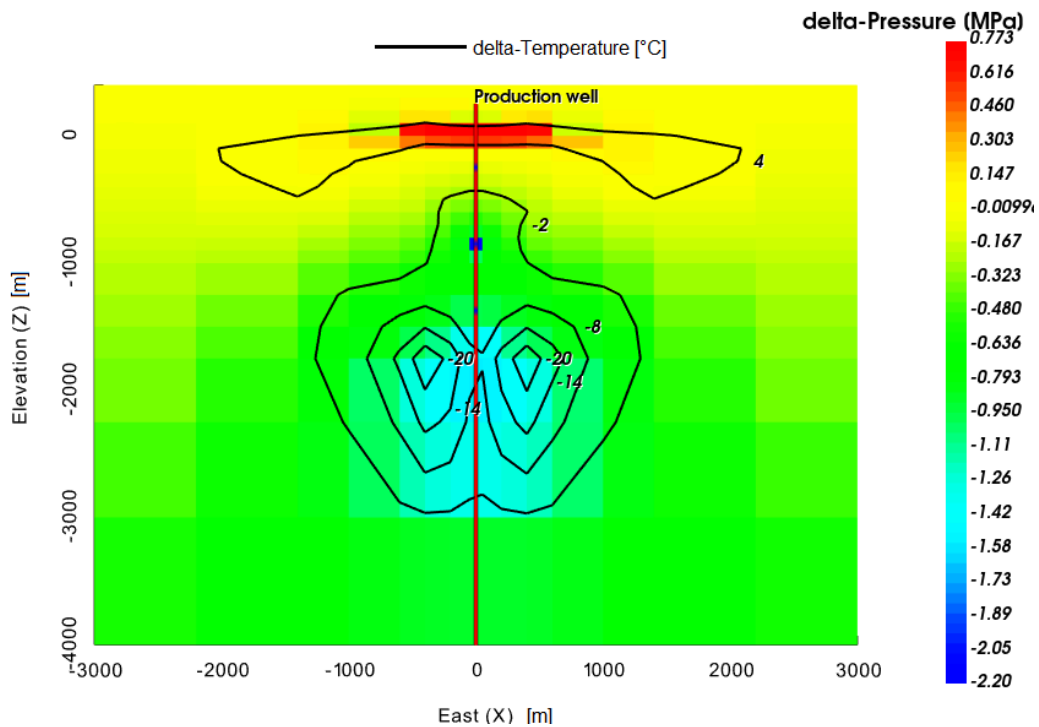


Figure 3.4.5. The pressure changes in the boiling reservoir and the accompanying temperature changes.

4. Discussion

The results give us a general idea on the effective lithological and effective production parameters controlling the discharge enthalpy in geothermal production. What remains to be explored is how these results hold up against data from geothermal fields. In this chapter we will discuss how the results compare to data from a few long running production fields and suggest follow up research.

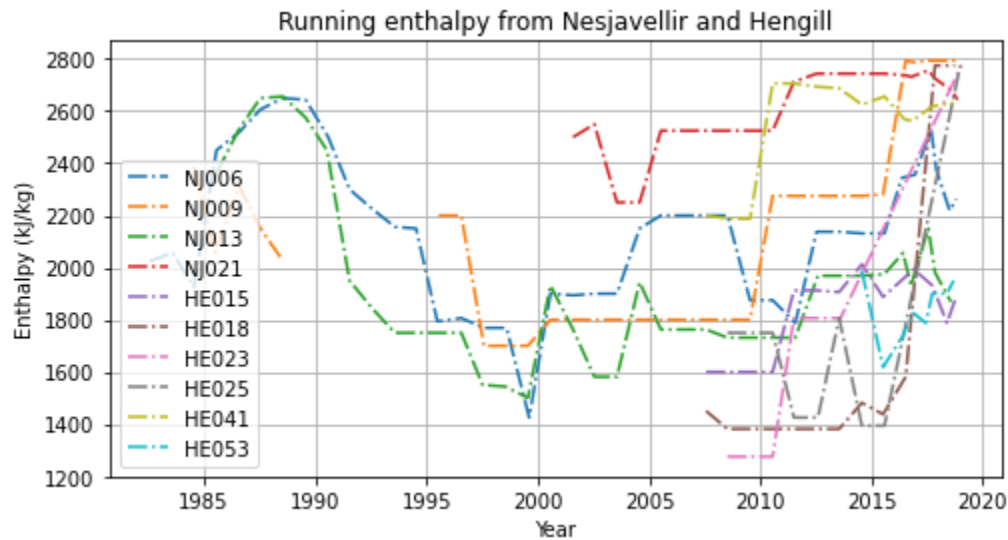


Figure 4.1 The running enthalpy of ten drill holes from the Nesjavellir/Hengill geothermal area in Iceland. (Adapted from Sandström, 2021)

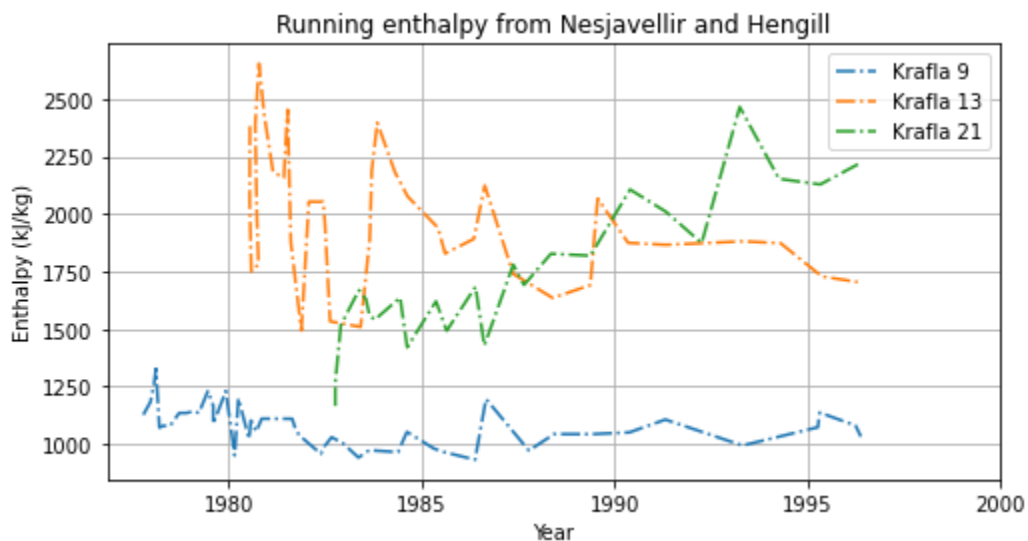


Figure 4.2 The running enthalpy of three drill holes from the Krafla geothermal area in Iceland (Adapted from Arnórsson & dAmore, 2000)

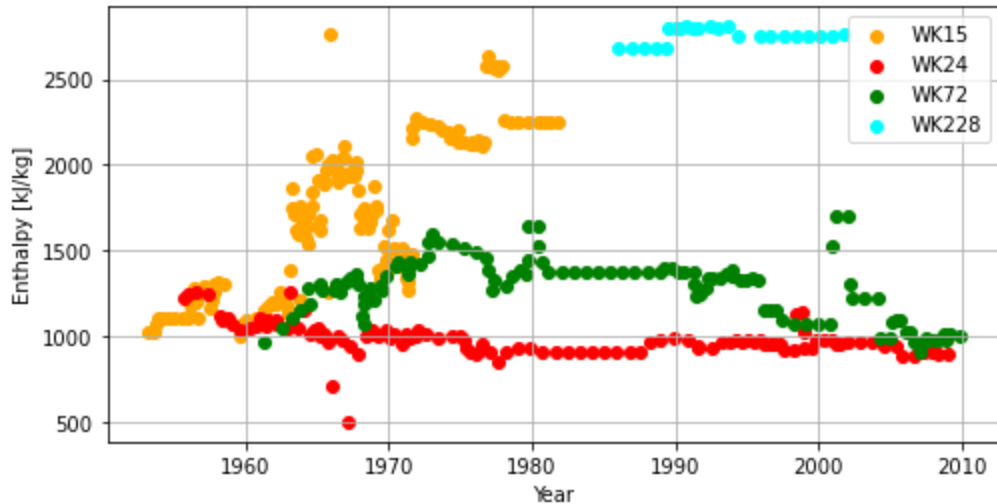


Figure 4.3 The running enthalpy of four drill holes from the Wairakei geothermal area in New Zealand. (Adapted from Yeh et al. 2015)

Enthalpy field data is somewhat hard to come by and requires a halt in a well's operation to conduct (**see section 1.1.2.**) along with being considered sensitive data on the business end of things. Taken as an example, available field data from the Nesjavellir, Hengill, Krafla and Wairakei geothermal fields (**figs 4.1 - 4.3.**) shows the extent to which production well enthalpy can fluctuate. With the operational history of many wells spanning decades, they provide a long, if sometimes low resolution production record. These records indicate both induced boiling from pressure drawdown of the field and enthalpy fluctuations in individual holes. The initial enthalpy is often low but slowly climbs to approaches saturated vapour values. That can be said for holes WK15 (**fig. 4.3**), NJ006 and NJ013 (**fig. 4.1**) where the enthalpy develops smoothly into $>2000 \text{ kJ kg}^{-1}$ before smoothly drawing down again similarly to the models in **figures 3.3.3 & 3.3.6**. Rapid spiking and subsequent depression such as the ones seen in low fracture permeability models (**figures 3.3.1, 3.3.5 and 3.3.8**) seem to be somewhat rarer in real life, although something of the sort occurs early in **Krafla 13**. This is most likely due to preference for wells that have more deliverability. Wells in minimally fractured zones will not be developed past the exploration phase, and therefore not monitored.

Comparing our simple model to field data, we see some consistency in the range of enthalpy fluctuations and other reservoir behaviour, although one can expect much more variability in field data and a much greater complexity behind it. In the liquid dominated model we develop a steam cap through depressurisation. Similarly, the Svartsengi geothermal field initially started off as a liquid dominated, high enthalpy field (Gudmundsson & Þórhallsson, 1986) but has since developed an extensive steam cap. Svartsengi has permeability of $<1e^{-13}$. Our model has an overall permeability somewhere in the range of Krafla, Nesjavellir or Baca (New Mexico). (Björnsson & Böðvarsson, 1990)

The apparently most sensitive parameter for EED is fracture permeability. Another mechanism for its development could be modelled, namely the choking of fractures as a result of production.

Two varieties of choking mechanisms could be considered for modelling. One would model fracture aperture as a function of reservoir pressure. As production draws down the fluid pressure, some fractures might contract. On the other hand, recirculation of waste fluid from the power plant may dilate fractures through increased pressure. The second alternative mechanism to be modelled is choking via mineral dissolution. As production draws in the fluid and induces boiling of the liquid fraction, minerals may start falling out of solution and subsequently choking the feeding fractures. These models, coupled with the work so far, could shed more light on the effective mechanisms and systematics behind EEDs.

5. Conclusions

Excess enthalpy discharges occur through at least two mechanisms under at least five conditions

1. Induced boiling.
 - a. From flashing around the feed zone.
 - b. From the pressure drawdown slowly invading the aquifer.
2. Phase segregation of liquid and vapour
 - a. Of pre-existing vapour in a boiling zone, these EEDs are usually long lived.
 - b. Of vapour slowly separating from the fluid mix in tight fractures ($\leq 15e^{-15} \text{ m}^2$) and being released in spikes of enthalpy.
 - c. A mix of the previous two processes.

The strength of phase segregation is controlled primarily by fracture permeability and the relative permeability curve. Secondary controls such as matrix permeability, matrix volume fraction, depth of feed-zone and fracture spacing can shift and stretch the running enthalpy curve; they can also affect spikes in enthalpy formed from flashing by changing their amplitude and frequency.

These mechanisms dictate the evolution path of the running enthalpy curve. In a boiling aquifer with intermediate fracture permeability ($1e^{-14} \text{ m}^2$), an initial flash produces a spike in enthalpy that drops after weeks to a couple of years, after which the pressure change will slowly invade the reservoir and induce further boiling which will make the enthalpy curve evolve in a parabolic manner, slowly rising and slowly receding over a few years to a decade before finally approaching the initial reservoir enthalpy. Tighter boiling reservoirs will also have a baseline enthalpy above that of the initial reservoir fluid. But have relatively rapid spiking enthalpy discharges with recovery periods where the enthalpy sometimes drops below the running baseline or even the initial reservoir fluid enthalpy. Sub-boiling reservoirs have a radically different evolution path where no excess enthalpy discharges occur in reservoirs with leakier fractures ($> 1e^{-15} \text{ m}^2$). For tight fractured sub-boiling reservoirs, the excess enthalpy discharges will take the form of rapid enthalpy spikes with longer periods of recovery.

Citations

Arnórsson, S. and D'Amore, F. (2000) Monitoring of Reservoir Response to Production. In: Arnórsson, S., Ed., *Isotopic and Chemical Techniques in Geothermal Exploration Development and Use: Sampling Methods, Data Handling, Interpretation*, International Atomic Energy Agency, Vienna, 309-341.

Austria, Jr, J.J.C. (2014). Dual porosity numerical models of geothermal reservoirs [Doctoral Thesis, The University of Auckland] <https://researchspace.auckland.ac.nz/handle/2292/27115>

Jemuel, J., Austria, C., O'Sullivan, M.J., & Vargas, J. (2015). Dual Porosity Models of a Two-phase Geothermal Reservoir. <https://pangea.stanford.edu/ERE/db/WGC/papers/WGC/2015/22004.pdf>

Björnsson, G. & Böðvarsson, G.. (1990) A survey of geothermal reservoir properties. *Geothermics 19 (1)*, pp. 17-27. [https://doi.org/10.1016/0375-6505\(90\)90063-H](https://doi.org/10.1016/0375-6505(90)90063-H)

Bjornsson, G., 2004. Reservoir Conditions At 3-6 Km Depth In The Hellisheidi Geothermal Field, Sw-Iceland, Estimated By Deep Drilling, Cold Water Injection And Seismic Monitoring. In: PROCEEDINGS, Twenty-Ninth Workshop on Geothermal Reservoir Engineering. Stanford, California.

Corey, A. T.: "The Interrelation Between Gas and Oil Relative Permeabilities", *Producers Monthly*, Nov. (1954), 38-41.

Darcy, H. (1856). *Les fontaines publiques de la ville de Dijon: Exposition et application.. Victor Dalmont.*

Franz, P. & Clearwater J. (2023). Volsung User Manual Version 1.20.20230603. Retrieved from: <https://www.flowstatesolutions.co.nz/documentation>

Fridriksson, Thráinn; Mateos, Almudena; Audinet, Pierre; Orucu, Yasemin. 2016. Greenhouse Gases from Geothermal Power Production. *World Bank*, Washington, DC. <http://hdl.handle.net/10986/24691>

Gebbru, T. N. (2023). Prediction of Injection-Induced Cooling using Tracer Test Data in the Hellisheidi Geothermal Field, SW Iceland Comparison of Numerical and Analytical Modelling Approaches [Master's thesis]. <http://hdl.handle.net/1946/43321>

Grant, M. A., & Bixley, P. F. (2011). Chapter 8—Production Testing. In M. A. Grant & P. F. Bixley (Eds.), *Geothermal Reservoir Engineering (Second Edition) (Second Edition, pp. 131–168). Academic Press.* <https://doi.org/10.1016/B978-0-12-383880-3.10008-3>

Gudjonsdottir, M., Palsson, H., Eliasson, J., & Saevarsdottir, G. (2015). Calculation of relative permeabilities of water and steam from laboratory measurements. *Geothermics*, 53, 396–405. <https://doi.org/10.1016/j.geothermics.2014.08.006>

- Gudmundsson, J.S.; Þórhallsson, S. (1986) The Svartsengi reservoir in Iceland. *Geothermics* 15(1) pp. 2-15. [https://doi.org/10.1016/0375-6505\(86\)90025-8](https://doi.org/10.1016/0375-6505(86)90025-8).
- Hayba, D. O., & Ingebritsen, S. E. (1997). Multiphase groundwater flow near cooling plutons. *Journal of Geophysical Research: Solid Earth*, 102(B6), 12235–12252. <https://doi.org/10.1029/97JB00552>
- IAPWS (2007). Revised Release on the IAPWS Industrial Formulation 1997 for the Thermodynamic Properties of Water and Steam. *The International Association for the Properties of Water and Steam*. <http://www.iapws.org/relguide/IF97-Rev.pdf>
- Ingebritsen, S. E., Geiger, S., Hurwitz, S., & Driesner, T. (2010). Numerical simulation of magmatic hydrothermal systems. *Reviews of Geophysics*, 48(1), RG1002. <https://doi.org/10.1029/2009RG000287>
- Johnson, D.M. (2006). Fluid permeability of oceanic basalts. Initial Rep. Deep Sea Drill. Proj., 68 (1980), pp. 1473-1477 Accessed via http://deepseadrilling.org/51_52_53/volume/dsdp51_52_53pt2_68.pdf
- Marini, L., & Cioni, R. (1985). A chloride method for the determination of the enthalpy of steam/water mixtures discharged from geothermal wells. *Geothermics*, 14(1), 29–34. [https://doi.org/10.1016/0375-6505\(85\)90091-4](https://doi.org/10.1016/0375-6505(85)90091-4)
- Pollack, H. & Hurter, S & Johnson, J. (1993). Heat Flow from the Earth's Interior: Analysis of the Global Data Set. *Reviews of Geophysics*. 31. 267-280. <https://doi.org/10.1029/93RG01249>
- Poux, B & Gunnarsdóttir, S & O'brien, J. (2019, September). 3-D Modeling of the Hellisheiði Geothermal Field, Iceland, using Leapfrog [Conference paper] Geothermal Resource Council 2019. https://www.researchgate.net/publication/356642614_3-D_Modeling_of_the_Hellisheiði_Geothermal_Field_Iceland_using_Leapfrog
- Pruess, K. (1992) Brief Guide to the MINC-Method for Modeling Flow and Transport in Fractured Media. United States. <https://doi.org/10.2172/6951290>
- Ratouis, T., Snæbjörnsdóttir, S., Gunnarsson, G., Ingvi, G., Kristjánsson, B., and Aradóttir, E. (2019). Modelling the Complex Structural Features Controlling Fluid Flow at the CarbFix2 ReInjection Site, Hellisheiði Geothermal Power Plant, SW-Iceland. 44th Workshop on Geothermal Reservoir Engineering, Stanford, California. <https://pangea.stanford.edu/ERE/db/GeoConf/papers/SGW/2019/Ratouis.pdf>
- Ratouis, T., Snæbjörnsdóttir, S., Voigt, M., Sigfússon, B., Gunnarsson, G., Aradóttir, E.S., and Hjørleifsdóttir, V. (2022). Carbfix 2: A transport model of long-term CO₂ and H₂S injection into basaltic rocks at Hellisheiði, SW-Iceland. *International Journal of Greenhouse Gas Control*, 114. <https://doi.org/10.1016/j.ijggc.2022.103586>
- Sandström, F. (2021). Evaluation of Relative Permeabilities and Excess Enthalpy Modeling for Geothermal Reservoirs [Master's thesis]. *Reykjavik University*. <http://hdl.handle.net/1946/39420>

- Schön, J. H. (2015) Physical properties of rocks. A workbook. *Elsevier*. ISBN: 978-0-444-53796-6
- Scott, S., Driesner, T., & Weis, P. (2016). The thermal structure and temporal evolution of high-enthalpy geothermal systems. *Geothermics*, 62, 33–47. <https://doi.org/10.1016/j.geothermics.2016.02.004>
- Scott, S. W. (2020). Decompression boiling and natural steam cap formation in high-enthalpy geothermal systems. *Journal of Volcanology and Geothermal Research*, 395, 106765. <https://doi.org/10.1016/j.jvolgeores.2019.106765>
- Stein, C. A., & Stein, S. (1992). A model for the global variation in oceanic depth and heat flow with lithospheric age. *Nature*, 359(6391), 123–129. <https://doi.org/10.1038/359123a0>
- Verma, A. K., 1986. Effects of Phase Transformation of Steam–Water Relative Permeabilities. Ph.D. thesis, University of California, Berkeley. <https://doi.org/10.2172/5540005>
- Wang, Y. and Pang, Z. (2022). Heat flux in volcanic and geothermal areas: Methods, principles, applications and future directions, *Gondwana Research*, <https://doi.org/10.1016/j.gr.2022.09.010>
- Yan, C. Y. (2022). *Introduction to Engineering Thermodynamics*. BC Campus. <https://pressbooks.bccampus.ca/thermo1/>
- Yeh, A., Boyce-Bacon, J., & O’Sullivan, M. (2015). *Review of Deliverability Models Used in Geothermal Reservoir Simulations*. Proceedings World Geothermal Congress 2015 Melbourne, Australia, 19-25 April 2015. <http://hdl.handle.net/2292/28108>
- Zarrouk, S. J., & McLean, K. (2019). Chapter 6—Completion and output testing. In S. J. Zarrouk & K. McLean (Eds.), *Geothermal Well Test Analysis* (pp. 113–154). Academic Press. <https://doi.org/10.1016/B978-0-12-814946-1.00006-2>
- Pórhallsson, S. (2003). Geothermal well operation and maintenance. *United nations university and ÍSOR*. <http://hdl.handle.net/10802/4798>